Ministry of Higher Education and Scientific Research

Kasdi Merbah Ouargla University

Faculty of New Information and Communication Technologies

Department of Electronics and Telecommunications

Dissertation

ACADEMIC MASTER

Domain : Sciences and Technologies

Branch : Telecommunications

Specialty "Systems of telecommunications"

Design of 2D PhC biosensor based on ring resonator for high precision detection of waterborne bacteria

Presented and publicly defended by

Farah Amna BOUGOFFA and Bouchra RAMDANI

On 02-06-2025

Jury

Boualem MEKIMAH,	MCA at Ouargla university	President
Mohammed BOULESBAA,	Professor at Ouargla university	Supervisor
Hamza OTMANI,	MCA at Ouargla university	Examinator
Rima HADJADJ,	PhD student at Ouargla university	guest

P
F
E

Dedication

In the name of God, the Most Gracious, the Most Merciful.

To my **affectionate mother**, whose prayers, love, and presence are the rhythm of every good day.

To **my father**, whose strength has always been a lantern on my path..

To **my sisters, nephews and all my family** , for the quiet support, the proud smiles, and the unwavering belief.

To **my teachers**, for knowledge freely given and doors opened wide.

And to the quiet source of strength, the gentle presence that never asked to be seen, but was always felt.

to all the silent contributions.

I dedicate this humble achievement to you all. May it carry a trace of every kind word, every silent prayer, and every quiet act of love.

Farah

Dedication

In the name of Allah, the Most Gracious, the Most Merciful

To my **beloved mother**, a constant source of comfort and prayers, whose warmth and quiet support accompanied me every step of the way, leaving a profound impact on everything I have achieved.

To my **dear father**, who taught me the values of patience and perseverance, and whose guidance and encouragement were a strong motivation to keep going.

To my **husband**, a true pillar of support, who stood by me through every difficult moment and meaningful milestone with unwavering devotion.

To my **precious family**—my brothers and sisters—for every proud moment and word of encouragement that added value to this journey.

To my **respected teachers**, who were beacons of knowledge and light, opening the doors of learning to me with great generosity.

I dedicate this humble achievement to you all. May it carry a trace of every kind word, every silent prayer, and every quiet act of love.

Bochra

Acknowledgements

We thank Allah the Almighty for giving us the courage, the will, the health, and the patience, so that, during all these years of study, we can get to where we are today and exploit all our efforts for this modest work.

We want to thank our supervisor, **Pr. Mohammed BOULESBAA**, professor at the University of Ouargla, for his kindness, his trust, his advice and his constant support to carry out this letter.
We thank the members of the jury **Dr. Boualem Mekimah** senior lecturer of Class A and **Dr. Hamza Otmani** class A senior lecturer for agreeing to evaluate this graduation work.

We would like to express to **Mrs. Rima Hadjadj**, PhD student at the university of Ouargla, all our gratitude for the honor she has done for us.

Our thanks are also addressed to our Department of Electronics and Telecommunications of the university of Kasdi Merbah Ouargla teachers for their contributions to our training.

Finally, we thank our families, our friends and all those who, from near or far, have contributed to the realization of this work.

Résumé

Dans ce mémoire, nous avons proposé, conçu et analysé deux structures d'un biocapteur à base de cristaux photoniques PhC-2D pour la détection de bactéries hydriques, en utilisant un seul anneau résonateur et l'autre structure basée sur des bi-anneaux résonateurs. Ces structures de biocapteur ont été réalisées sur un réseau formé de tiges circulaires de silicium d'indice de réfraction 3,48 IUR, dans un fond d'air d'indice 1 IUR. Nous avons calculé la bande interdite photonique par la méthode PWE, et analysé la transmission à l'aide de FDTD. Dans notre projet, nous avons étudié la détection, la présence des différents types de bactéries dans l'eau contaminée, à savoir V.cholera, E.coli, S.flexneri et S.flagellin. Le facteur de qualité le plus élevé obtenu est 1569.4 et le facteur de mérite a atteint 163.65(RIU^{-1}) pour E. coli (RI = 1.388). La sensibilité maximale était de 151.54 nm/RIU pour S. flagellin (RI = 1.43), et la limite de détection minimale atteinte est $6,1 \times 10^{-4}$ RIU.

Mots-clés: biocapteur ; cristaux photoniques ; tiges de mesure ; facteur de qualité ; sensibilité ; PWE ; FDTD

Abstract

In this dissertation, we proposed, designed and analyzed novel 2D photonic crystal (PhC-2D) biosensor structures for identifying waterborne bacteria based on a ring resonator. The structures were designed with an array of circular silicon rods with a refractive index of 3.48 RIU, in an air background with a refractive index of 1 RIU. We calculated the photonic bandgap using the PWE method and the transmission power of the proposed biosensors was evaluated using the FDTD method. We were interested in studying the detection of bacterial contamination in water, and relied on some important variations in the structure's parameters to maximize the biosensor sensitivity. The quality factor was at a maximum of 1569.4 and the factor of merit was up to 163.65 (RIU^{-1}) for E. coli (RI = 1.388). The sensitivity was the highest at 151.54 nm/RIU for S. flagellin (RI = 1.43), and the optimal detection limit achieved was 6.1×10 RIU.

Keywords: biosensor; photonic crystals; measuring rods; quality factor; sensitivity; waterborne bacteria; FDTD

ملخص

في هذه الدراسة ، قمنا باقتراح وتصميم وتحليل ومحاكاة بنى سداسية جديدة لجهاز استشعار حيوي على أساس البلورات الفوتونية الضوئية $CPs-2D$ للكشف عن البكتيريا المنقولة عبر المياه. تم تنفيذ هذا العمل بتوزيعات دائرية لقضبان السيليكون مع معامل انكسار 3.48 RIU ، في خلفية هوائية. يتم حساب فجوة النطاق بطريقة (PWE) ، وتم تحليل نتائج المحاكاة باستخدام طريقة (FDTD). لقد عملنا على تطبيق اكتشاف التلوث البكتيري في الماء بهيكلين مختلفين لمقارنة الهياكل ذات التجويف الفردي والهياكل ثنائية التجويف. في النتائج ، يمكننا أن نرى عامل جودة أفضل مع الهيكل المصمم بتجويفين هو 1569.4 ، وحساسية عالية في الهيكل الثاني 151.54 نانومتر / RIU . عند طول موجة يبلغ حوالي 1400 نانومتر ، والتي تتحول مع التغير في معامل الانكسار ، عندما يتغير من 1 إلى 1.446 RIU ، توجد علاقة عكسية بين الهيكلين فيما يتعلق بأقصى شدة من طيف الإرسال. بتعبير أدق ، تنخفض الكثافة القصوى للهيكل أحادي التجويف ، بينما تزداد في الهيكل الثاني.

الكلمات المفتاحية : جهاز استشعار حيوي ؛بلورات فوتونية؛ جزيئات محددة؛ معامل الانكسار فجوة الفرقة؛ PWE ؛ FDTD .

Contents

List of figures

List of Tables

List of abreviations

PBG	Photonic Bandgap.
P*h*C	Photonic Crystal.
PC*s*	Photonic Crystals.
2D	Two-Dimensional.
3D	Three-Dimensional.
FDTD	Finite-Difference Time-Domain method.
PWE	Plane Wave Expansion method.
PML	Perfectly Matched Layer.
TE	Transverse Electric, TE polarization.
TM	Transverse Magnetic, TM polarization.
SPR	Surface Plasmon Resonance.
LD	Limit of Detection.
Q	Quality factor.
S	Sensitivity.
RIU	Refractive Index Unit.
FOM	Figure of Merit.
si	silicon.
S.$flexneri$	Shigella flexneri.
S.$flagellin$	Salmonella flagellin.
V.$cholera$	Vibrio cholera.

List of symbols

λ	Wavelength.
λ_0	Resonant wavelength.
a	Photonic crystal period
r	Photonic crystal radius
f	Air filling factor
R	The reflectivity
n	Refractive index.
c	Speed of light in vacuum
ϵ	Dielectric permittivity
V	The potential.
vi	Volume occupied by the material of permittivity
Λ	Volume of the cell.
Δ_n	Refractive index contrast.
E	The electric field.
H	The magnetic field
K	The direction of the reciprocal network corresponds to the direction of the first

General introduction

Waterborne diseases continue to be one of the biggest health problems worldwide, affecting millions of people in both developing and developed countries. These diseases mainly happen because people consume water contaminated with tiny organisms like bacteria, viruses, and parasites. The World Health Organization reports that about 80% of infectious diseases in developing countries come from unsafe water and poor sanitation, causing serious illnesses such as cholera, dysentery, typhoid fever, and chronic diarrhea [1]. The most common bacteria found in polluted water include Vibrio cholerae, Escherichia coli, Shigella flexneri, and Salmonella flagellin and other waterborne diseases [**?**]. What's even more worrying is that diarrhea caused by contaminated water kills more children under five than malaria, Acquired Immune Deficiency Syndrome (AIDS), and measles combined is roughly one child dies every minute because of this [2]. These numbers show how important it is to have fast and effective systems to detect water contamination early, so we can prevent outbreaks and protect people's health. Traditional detection methods like polymerase chain reaction (PCR) [3] and enzyme-linked immunosorbent assay (ELISA) [3]are widely used, but they tend to be slow, expensive, and require specialized labs and equipment. This makes them less practical for real-time or on-site testing [3,4]. This is where photonic crystal-based optical biosensors come in as a promising alternative. They offer many benefits such as high sensitivity, the ability to detect contaminants without chemical labels,real-time results, and only need a small amount of sample [5, 6]. The idea of photonic crystals was first introduced by Eli Yablonovitch in 1987. He described them as structures with a repeating pattern that control how light travels through them, similar to how semiconductors control electrons [7]. Photonic crystals work with the photonic band gap, which is a range of light frequencies that cannot pass through due to the repeating structure of materials with different refractive indices. When a defect layer is added inside this structure, it creates a special resonance that can be detected when something changes inside,like bacteria entering the water [8, 9]. These crystals come in different forms: one-dimensional (1D),two-dimensional (2D),and three-dimensional (3D). The 2D type is the simplest and cheapest to make, which makes it ideal for practical uses [10]. In our study,we propose designing a 2D photonic crystal biosensor with a silicon (Si) defect layer to detect changes in refractive index caused by bacteria in water,such as V. cholera (n = 1.365),E. coli (n = 1.388),S. flexneri (n = 1.422),and S. flagellin (n = 1.430),compared to pure water (n = 1.333) [11]. Using the finite difference time domain (FDTD) method, we analyze how the PhC biosensor's transmission spectrum changes,measuring how sensitive it is to shifts in wavelength caused by refractive index variations.

This work is divided into four main chapters,each focusing on a key stage in the design and analysis of an optical biosensor based on photonic crystals:

Chapter one covers the theoretical background of the photonic crystals. First,it will present the different types of the photonic crystals and their main properties. It also highlights their various applications, especially in the field of biomedical detection.

Chapter two focuses on the applications of the photonic crystals in the field of biosensing. It will also describe the various optical performance parameters of the PhC biosensors including quality factor, sensitivity, FoM. The process techniques for manufacturing biosensors based on photonic crystals will also be discussed.

Chapter three is the core of the project. It presents the actual design of a biosensor based on a hexagonal photonic crystal structure with a single cavity. This cavity traps light,and when biological molecules enter it,the light's behavior changes—allowing detection. The chapter explains the design steps, the materials used,and how the crystals are arranged. It also uses simulation tools to analyze the optical performance of the sensor and optimize it for better sensitivity and accuracy.
Chapter four complements the work presented in the previous chapter by proposing an improved version of the biosensor. This time,the hexagonal photonic crystal structure incorporates two cavities instead of just one. This choice allows for better confinement of light and amplifies the changes observed when biological molecules enter the sensor,which improves detection accuracy. This chapter details the different design stages of this new architecture,the chosen materials, as well as the arrangement of the photonic crystals and cavities. FDTD simulation method is also used to analyze the optical performance of the sensor and optimize it in terms of sensitivity and selectivity,while taking into account the coupling effect between the two cavities. Through this dissertation, we aim to develop optical biosensors based on 2D photonic crystals, capable of accurately detecting the presence of biomolecules.
In conclusion, we will close this dissertation with a general summary that will highlight the work carried out and future prospects.

Chapter 1

Introduction to photonic crystals: presentation & applications

Contents

1.1 Introduction

Introduction In recent years, photonic crystals have acquired great importance thanks to their ability to control light propagation on the wavelength scale. Thanks to their periodic structure, these materials generate photonic band gaps, enabling light to be precisely directed and manipulated, paving the way for innovative applications in a variety of technological fields.

In this chapter, we provide a comprehensive introduction to photonic crystals, exploring their fundamental characteristics and examining the different types of crystals that exist.

We will also discuss the importance of defects within these crystals, which can be exploited to design high-performance optical devices. Finally, we will present some varied applications of photonic crystals, focusing on their use in optical telecommunications and integrated optics, with a particular focus on the application of power dividers based on photonic crystals [12].

1.2 Definition

Photonic crystals are materials whose dielectric permittivity is periodically modified on a scale comparable to or smaller than the wavelength of light. As illustrated in figure 1.1, the periodicity can be one-dimensional (1D), two-dimensional (2D) or three-dimensional (3D), giving rise to a phenomenon known as Photonic Band Gaps. These bands represent a range of optical frequencies in which light waves cannot propagate through the material. Photonic crystals exhibit unique properties resulting from the interaction of light with the periodic structure of the refractive index, making them promising tools in the fields of optics and photonic electronics. These materials can be fabricated using modern techniques such as nanometric printing or laser etching, and are not limited to a specific type of material, enabling the use of a variety of materials, including insulators, semiconductors and even metals [13].

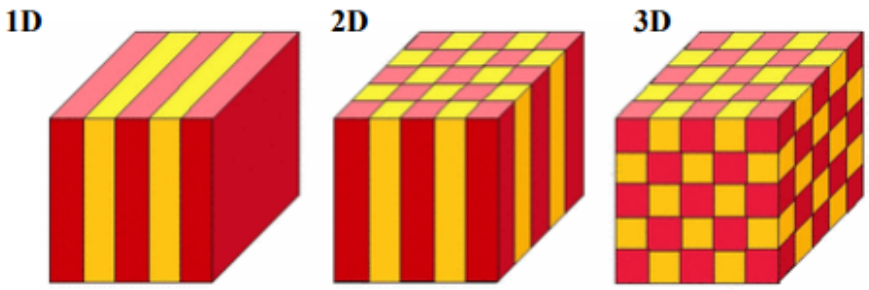

Figure 1.1: Various photonic crystal structures of different dimensions.

1.3 Natural photonic crystals

Photonic structures have existed in nature for millions of years. Colors play an essential role in the communication of living beings, be they animals, plants or even minerals. This

effect is not limited to appearance, but also contributes to survival and reproduction [14].

1.3.1 Butterflies

Butterflies are among the most fascinating insects, thanks to their brilliant colors. They are highly dependent on light and use incredible mechanisms to interact with it to their advantage. For example, the Cyanophrys acaste butterfly, native to Brazil, owes its magnificent blue and green reflections to the interaction of light with the microscopic structure of its wings (see figure 1.2). A closer look reveals a network of holes arranged in an almost hexagonal pattern, as illustrated in the figure1.3, creating this spectacular color effect [12].

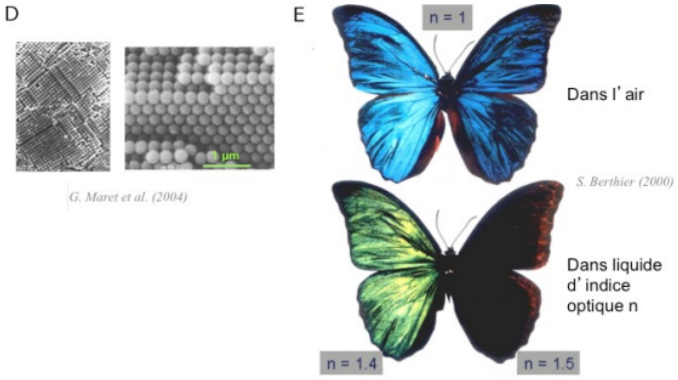

Figure 1.2: Examples of artificial photonic crystals

1.4 Different types of photonic crystals

Photonic crystals vary according to their dimensionality and can be classified into the following categories:

1.4.1 One-dimensional (1D) photonic crystals

These structures are commonly referred to as Bragg gratings. They consist of alternating flat dielectric layers of thickness $\lambda/4$, where λ represents the wavelength guided in the material. They are generally made by stacking layers of different refractive index and optical thickness. One-dimensional photonic crystals are obtained by stacking layers of different dielectric indices. These structures are composed of the periodic alternation in a single direction in space of two dielectric media of respective dielectric constants [15].

The applications of one-dimensional photonic crystals:
-Convertisseurs modes for optical fibers.
-Filtres wavelength-selective.
- Multiplexeurs [15].

$$\Delta_n = n_h - n_1 \tag{1.1}$$

with :
n_h : The refractive index of the high index material.
n_1 : The refractive index of the low index material.

1.4.1.1 Bragg gratings

Bragg gratings are composed of periodically stacked layers with different refractive indices. When a light wave passes through this structure, it undergoes reflections at each interface between two layers. If the light passes from a low-index medium to a higher-index medium, a phase shift of π occurs ,in the opposite case, no phase change takes place. When the optical thickness of the layers is chosen to be equal to half the wavelength (λ/2), the waves reflected by the different interfaces will interfere constructively. This means that they reinforce each other, leading to almost total reflection of the light. This phenomenon then prevents light from propagating through the structure, giving rise to a photonic band gap (or PBG) As seen in the figure 1.4 , i.e. a range of frequencies where light cannot propagate [16].

$$a = (a_1 + a_2) \tag{1.2}$$

with :
a_1 : the thickness of the layer of index n_1.
a_2 : the thickness of the layer of index n_2.

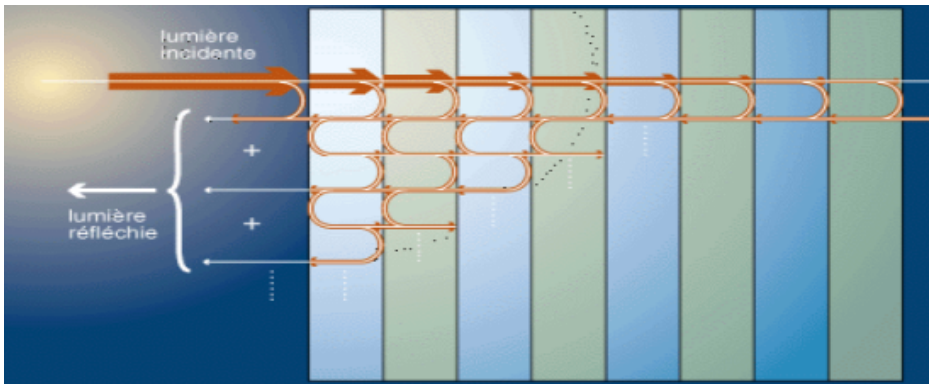

Figure 1.3: Periods of a one-dimensional photonic crystal.

1.4.2 Geometric and physical properties of a CPs-1D

The filling factor (f) is defined as being the ratio between the volume occupied by this material in the elementary cell of the crystal and the volume of the elementary cell.

For a planar two-dimensional photonic crystal composed of air holes drilled in a dielectric matrix, the air filling factor f designates the ratio between the area of the pattern and the area of the elementary cell of the network considered [15].

$$f = \frac{\mathrm{A}_{pattern}}{\mathrm{A}_{elementary.pattern}} \tag{1.3}$$

1.4.3 Index contrast

Ratio between the indices of the two materials, which can be compared to the height of the potential barrier in solid state physics [17].

$$\Delta_n = n_h - n_1 \tag{1.4}$$

with :
n_h : The refractive index of the high index material.
n_1 : The refractive index of the low index material.

1.4.3.1 Periods

These geometrical parameters, chosen according to the frequency range under study, influence the characteristics of the photonic bandgap.

For example, for a one-dimensional photonic crystal, the period a=(a1+a2) where a1 is the thickness of the first permittivity layerϵ_1 and a2 the thickness of the second permittivity layer ϵ_2

1.4.3.2 The filling factor f

can be compared to the width of the periodic potential, if taken for the high-index material, for example, it is defined as the ratio between the volume occupied by this material in the elementary cell of the crystal and the cell volume of the latter.

The influence of these different parameters on the behavior of a photonic structure can be understood by analogy with a periodic potential induced by the arrangement of atoms in a semiconductor [12].

$$\int = \frac{\mathcal{W}}{\Lambda} \tag{1.5}$$

With:

$\mathcal{W}$: Volume occupied by the material of permittivity ε_i

Λ: Volume of the cell.

1.5 Two-dimensional photonic crystals (CPs -2D)

A two-dimensional photonic crystal is a structure characterized by periodic modulation of dielectric permittivity in two directions in space, while being homogeneous in the third direction. The optical properties of two-dimensional structures (as well as those of one-dimensional structures at oblique incidence) depend strongly on the polarization of the electromagnetic wave.

There are a number of ways to manufacture these two-dimensional structures. For example, dielectric pillars can be placed in air or another dielectric medium, To achieve wide photonic band gaps, a high refractive index contrast (difference between the refractive indices of the medium and the pillars) is required. In addition, a material with two-dimensional Photonic Band gaps (PBGs) can also consist of a network of holes cut into a dielectric material. The optical responses of these structures are polarization-dependent and may not exhibit a complete band gap. A complete band gap means that the structure prevents the propagation of light in all directions of the periodicity plane, regardless of wave polarization [18].

1.5.1 Different families of two-dimensional photonic crystals

Two-dimensional periodic gratings can be grouped into three main families: [19]

1.5.2 Square grating

The grating nodes are located on side “a” fgure1.4. It has been shown that this type of grating is very sensitive to the angle of incidence and polarization of the electromagnetic wave. It is therefore difficult to obtain a total band gap, i.e. a band gap that prevents propagation whatever the polarization [19].

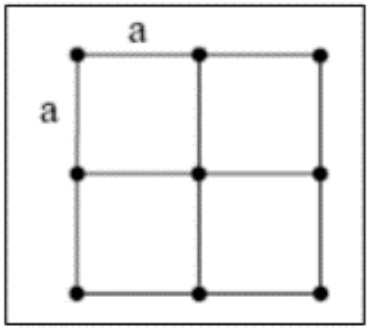

Figure 1.4: The square lattice.

1.5.3 Triangular lattice

The triangular lattice is the 2D lattice with the highest symmetry, as long as we limit ourselves to a single atom per mesh. Each lattice node is spaced from its nearest neighbor by the same distance “a” figure1.5. This structure is less sensitive to the angle of incidence than the square lattice, but the full band gap is still difficult to obtain [19].

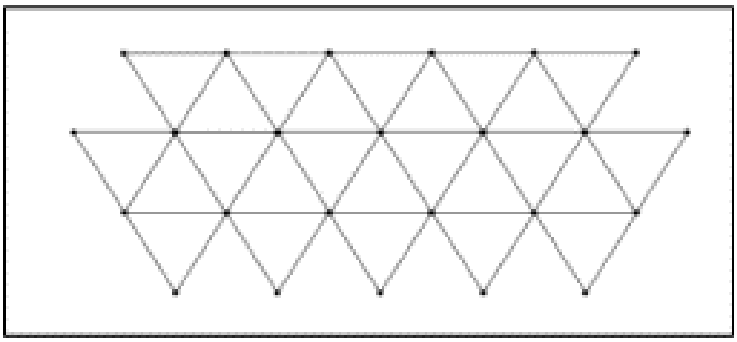

Figure 1.5: The triangular lattice.

1.5.3.1 Hexagonal lattice

On a hexagonal lattice, if all the neouds are identical and spaced by “a” (figure1.6), then this structure is called “graphite” because it is similar to the crystalline structure of graphite [19].

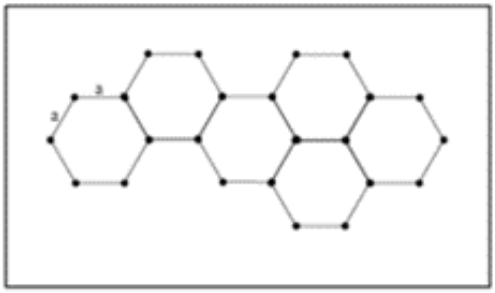

Figure 1.6: Hexagonal lattice example.

1.5.4 Boron nitride structure:

This structure provides a wide bandgap (figure1.7), and has the same structure as the hexagonal lattice, only one of the nodes differs in crystalline nature from boron nitride [19].

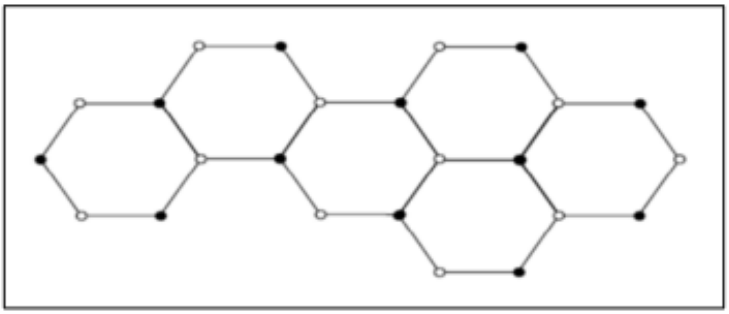

Figure 1.7: The boron nitride structure.

1.6 Three-dimensional photonic crystals (CPs-3D)

3D photonic crystals are the only structure that can achieve an energy bandgap in all spatial directions. The first three-dimensional photonic crystal and consisted of silicon spheres arranged in a diamond structure,But history generally retains the famous Yablonovite, a 3D microwave structure fabricated in 1993 by E. Yablonovitch by drilling holes in Plexiglas at three azimuthal angles 120 apart. Numerous manufacturing methods for three-dimensional photonic crystals have been proposed. The following two have attracted the most research effort [18]. nodes differs in crystalline nature from boron nitride.

1.7 Polarization of the electromagnetic wave (TE and TM)

properties of electromagnetic waves depend on the type of polarization (TE and TM). In the case of Transverse Electrical (TE) polarization, the electric field (E) is oriented in the periodicity plane, while the magnetic field (H) is perpendicular to this plane. In Transverse Magnetic (TM) polarization, on the other hand, the roles of the electric and mag-

netic fields are reversed. These differences give rise to distinct band gaps for each polarization. To achieve a total band gap that prevents light propagation in all directions, it is necessary for these band gaps to overlap, enabling complete control of light flow through the crystal as illustrated in the figure1.8 [20].

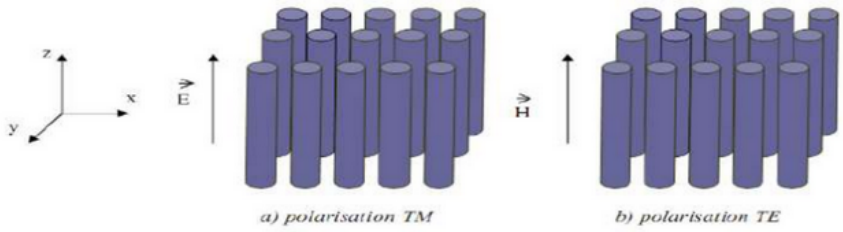

Figure 1.8: Representation of TE and TM polarizations in a 2D photonic bandgap (PBG).

1.7.1 Band diagram

Each photonic crystal has its own band diagram (figure 1.9) Using the plane-wave decomposition (PWE) method, we were able to obtain the band diagrams for the TE and TM modes of a photonic crystal consisting of a triangular grating etched into a heterostructure on a Si substrate, with a fill factor of 30%. In the case of the triangular grating, a photonic bandgap (BIP) is observed for TE polarization in the range u = 0.21-0.27, while no bandgap appears for TM polarization. On the other hand, in the case of the square grating, no photonic band gap is observed for either TE or TM polarization, As illustrated in the figure1.9. In general, TE bandgaps appear mainly for connected structures, while TM bandgaps are more favored in isolated structures, as is the case for pillars surrounded by air. Thus, the greatest BIP is obtained in the triangular array of air holes in a dielectric for TE polarization [20].

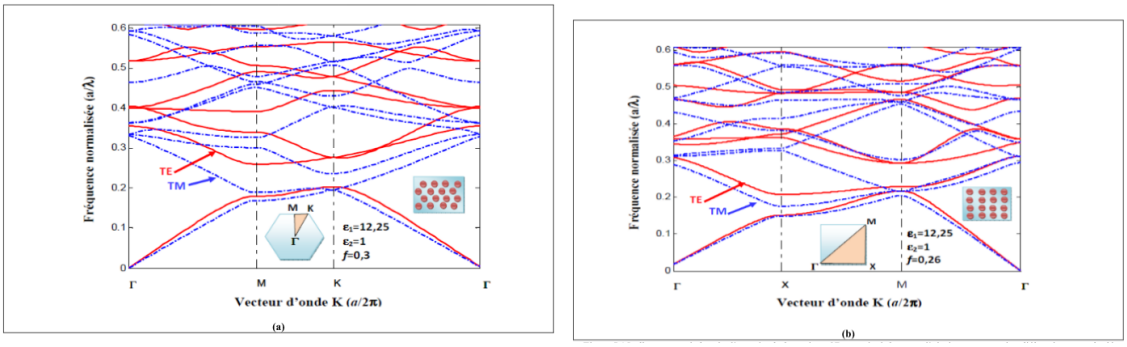

(a) (a) (b) (b)

Figure 1.9: Band gap maps of an array of air holes in a dielectric matrix: (a) Triangular lattice; (b) Square lattice.

1.7.2 Maps of forbidden bands

Bandgap maps show the position of the bandgap as a function of the fill factor f. For a square grating, the TE and TM band gaps open at f = 35 and f = 50 respectively. In the case of a triangular lattice, these bands appear at f = 11 and f = 63 respectively. The full bandgap region corresponds to the intersection of the TE and TM bandgaps, and lies within the $u = 0.37 - 0.56$ energy window. The triangular lattice is generally preferred to the square lattice, as the TE bandgaps are wider and open at lower filling factors illustrated in the figure1.10 [16].

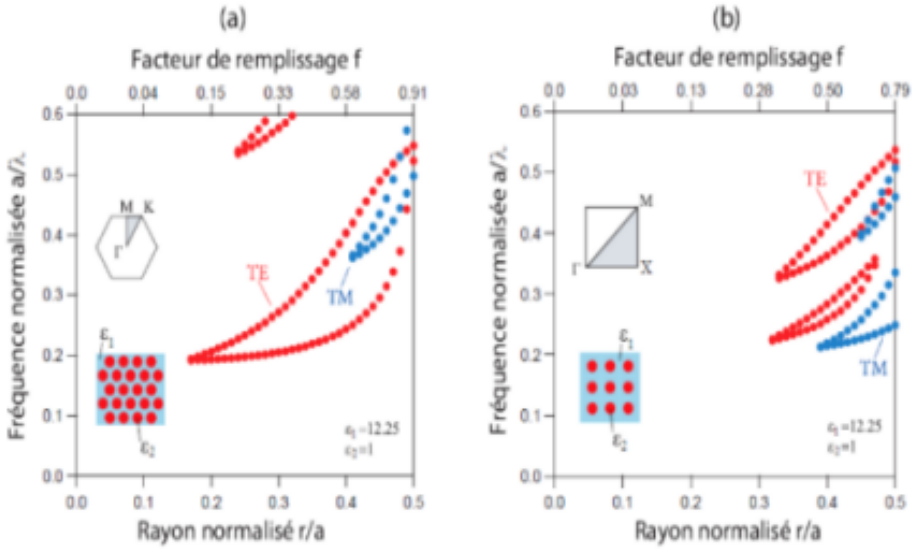

Figure 1.10: Band gap maps of an air-hole lattice in a dielectric matrix. (a) Triangular lattice; (b) Square lattice.

1.8 Different types of defect

Defects in photonic crystals can be exploited to create advanced optical applications, such as high-selectivity filters, where only electromagnetic waves with a frequency corresponding to a mode allowed in the bandgap can be transmitted. Among these defects, point defects are particularly important: they enable high-quality optical cavities to be formed by removing certain columns or lines in the crystal lattice, thus creating a localized mode capable of trapping light. It is also possible to create linear defects, known as waveguides, which allow light to be directed along defined paths within the crystal. As in semiconductors, these defects introduce permitted energy levels within the bandgap, paving the way for precise control of light propagation in these structures [21].

1.8.1 Point defects

photonic crystals, there are several ways to create point defects, such as by removing, adding, or modifying certain parts of the crystal pattern, These defects create optical cavities, and the resonant modes will position themselves within the forbidden bands of the crystal. The figure 1.11 shows the calculated transmission spectrum for a 2D crystal with

hexagonal symmetry, composed of dielectric rods, where the defect results from a missing rod. Although the transmission spectrum is almost identical to that of the defect-free crystal, with a band gap between 900 and 1300 nm, the addition of the defect generates a narrow and unique transmission peak at 1100 nm. This shows that we are dealing with a unimodal cavity, especially if we limit ourselves to a two-dimensional system. However, the idea of a unimodal cavity makes perfect sense in three-dimensional systems. With recent advances in the fabrication of 3D photonic crystals, the addition of size controlled defects to create true unimodal cavities has now become an achievable goal [21].

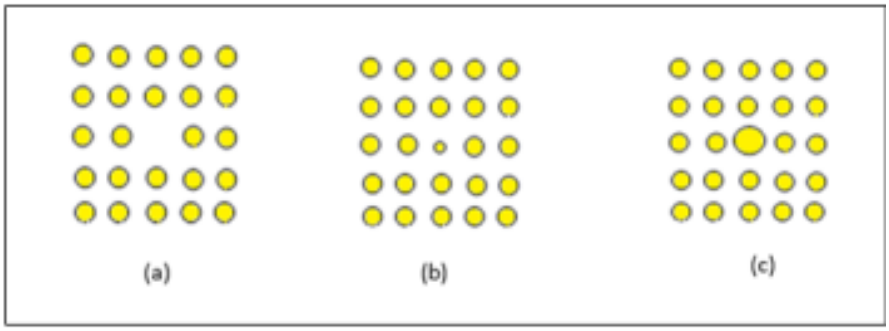

Figure 1.11: Examples of simple one-time defects. (a) Deficiency. (b) Atom in interstitial position.(c) Atom in the substitutional position.

1.8.2 Linear defects

Linear defects are defects used to guide waves, often referred to as extended defects. These defects can exist in three forms depending on the dimensions (1D, 2D, or 3D), but they can only be obtained in crystals with these dimensions. Among these defects, one-dimensional defects (w1) are the most studied and used, as they serve as guides for light within a photonic crystal. It is also possible to imagine Two-dimensional (W2) or even three-dimensional (W3) defects, which consist of several W1 guides aligned in different directions, thus allowing the transport of light along multiple paths within the crystal. The basic example is that of the linear waveguide W1 in a 2D photonic crystal. To create such a waveguide, point defects that are coupled and regularly spaced in a given direction of the 2D crystal are placed. The coupling between these resonators creates a permitted propagation band in the direction of the alignment. This type of coupled resonator waveguide was proposed in 1999

1.8.3 Photonic crystal waveguides

Photonic crystal waveguides direct light by introducing linear defects in the crystal structure that confine light within the photonic bandgap. Transmission can be enhanced by adjusting the size and shape of holes at bends or junctions. Although straight waveguides may experience significant losses, specially designed bent waveguides with angles of 60° or 120° help ensure efficient light transmission over a wide frequency range.

1.8.4 Photonic crystal splitter

The photonic crystal splitter efficiently divides and distributes light with low losses through waveguides connected at 120° angles. Its Y-junction design supports multiple

outputs and offers a flat spectral response across a wide wavelength range.

1.8.5 Directional coupler

A directional coupler connects two parallel waveguides to efficiently split or combine optical signals. A biosensor detects biological responses and converts them into electrical signals for analysis, with applications in medicine, environment, and food safety, providing fast and accurate results [22].

1.8.6 The Filter

A filter is a device or component designed to select or separate a specific range of wavelengths or frequencies from an optical or electrical signal, while blocking others. In optics, filters are used to control light by allowing certain colors to pass through and blocking others, enabling precise signal separation or modification in communication and sensing systems [23].

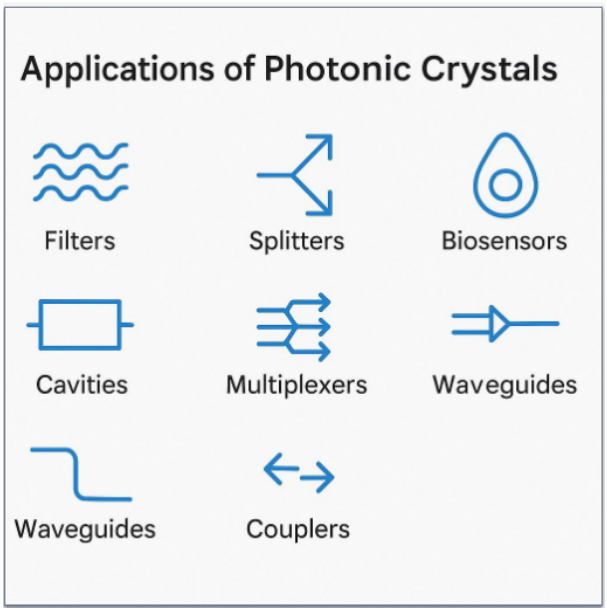

Figure 1.12: Applications of photonic crystals

1.9 Conclusion

Photonic crystals are innovative materials offering limitless possibilities to control light at very fine levels, by exploiting their periodic structure that generates photonic band gaps. These unique characteristics allow for advanced control or filtering of light, thus opening up vast prospects in numerous technological applications [17]. In this chapter, we covered the basics of photonic crystals, including their properties, different types, and multiple applications in fields such as optical fibres, sensors, and integrated optics [18, 24]. We also highlighted the importance of defects in these crystals, which can be exploited to develop innovative optical functions [25]. Thanks to this foundational knowledge, researchers and engineers can use photonic crystals to develop high-performance optical devices.

Chapter 2

Overview of photonic crystal sensors

Contents

2.1 Introduction

In today's healthcare, finding new ways to catch diseases early matters a lot. Old methods like ELISA tests, PCR, and different scans help doctors find illnesses. But these ways can be hard, slow, and need skilled workers. These problems make people look for new ways to spot diseases fast, easy, and cheap. One new tool is the Two-Dimensional Photonic Crystal (2D PhC) biosensors. They are small, have great light features,and can check things without delay.

Photonic crystals are special structures that change how light moves. They stop light from passing through certain frequency ranges. This helps control light at tiny scales, which is good for sensing things like proteins or diseases. When a target molecule like a protein or DNA hits the sensor, it changes the local refractive index. This shifts the photonic band structure, changing how the sensor responds. So, 2D PhC sensors can find tiny amounts of disease markers. This helps find diseases like cancer, infections, or brain issues early [18].

A main perk of 2D PhC biosensors is their flexible design. You can tweak things like grid size, hole size, and what stuff they're made of to make them work at set light waves and hit desired sensitivity levels. This lets us make special tools that can find many different substances. Plus, their flat and small shape makes them great for putting into lab-on-a-chip systems, pushing forward the creation of portable, efficient tools for quick health tests [26].

2D PhC biosensors work mainly by resonance shift and guided-mode methods. When a molecule connects with the surface of the photonic crystal, it causes a small change in refractive index, which moves the resonance wavelength. This move can be measured accurately using optical tools like spectroscopy or imaging. Guided-mode helps keep the light inside the sensor better, raising sensitivity and improving how well we hear the signal against the noise [27].

2D PhC biosensors have many strong points. But moving them from lab to clinic has hurdles. Making them is complex and pricey. Surface biofunctionalization and reproducibility add to this. New methods like electron beam lithography, nanoimprinting, and self-assembly help in easing some of these issues. Yet, more work is needed for better scaling and to cut costs even more [18].

2.2 Definition of a Sensor

The sensor is the first episode of the measurement series. It acts as a power converter byinteracting with a specific amount of material it wants to measure and characterize, andproviding a usable amount of material, which must be measured, such as electricalvoltage, frequency, intensity and deviation. External influencers such as temperature,humidity, chemical concentrations, etc, as seen in Figure 2.1.

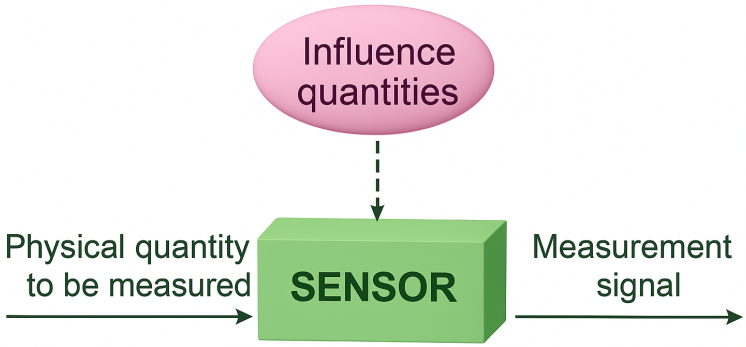

Figure 2.1

Figure 2.1: Principle of a sensor.

The different components of the sensor are described below and illustrated in Figure 2.2 :

- Test body: element that selectively responds to the measured quantity. It transforms a measured quantity into another measurable physical quantity.
- Transducer: Converts the responses of the test body into an electrical quantity constituting an output signal.
- Transmitter: element that amplifies, filters and improves the output signal for remote transmission. It may or may not be integrated into the sensor.

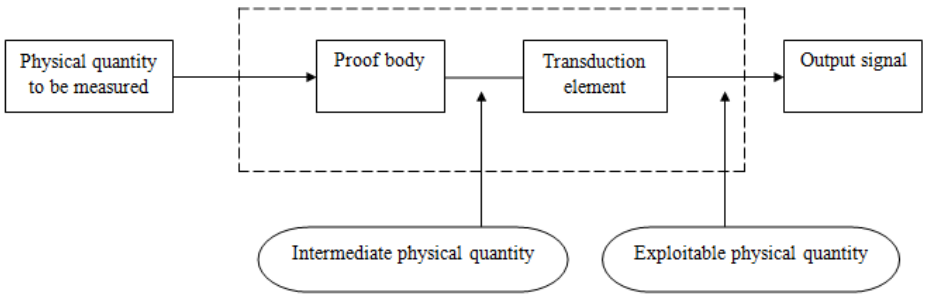

Figure 2.2: Constitution of a sensor.

Figure 2.3: A diagram showing the different types of biosensors classified.

2.3 Basic characteristics of the biosensor

There are certain static and dynamic characteristics that every biosensor has. Optimization of these properties is reflected in the performance of the biosensor:

2.3.1 Reproducibility

Reproducibility is the ability of a biosensor to generate identical responses for a duplicate experimental system. Repeatability is characterized by the precision and accuracy of the transducer and electronics in the biosensor. Precision is the ability of the sensor to provide identical results every time a sample is measured, and accuracy indicates the ability of the sensor to provide an average value close to the true value when the sample is measured more than once. Repeatable signals ensure high reliability and robustness of conclusions drawn from the biosensor response.

2.3.2 Stability

The biosensing system's stability refers to how susceptible it is to external perturbations both inside and outside of it. The output signals of a biosensor under measurement may wander as a result of these disruptions. This may result in a measurement mistake in the concentration and compromise the biosensors accuracy and precision. In situations when a biosensor needs to be continuously monitored or undergo lengthy incubation phases, stability is the most important characteristic. The sensitivity or detection limit (DL) of a biosensor is defined as the lowest concentration of an analytical material that it can detect. in several applications for monitoring the environment and medicine. As a result, sensitivity is a crucial biosensor characteristic. Linearity is an attribute showing the accuracy of the measured response to a straight line, mathematically represented in equation 2.1:

$$y = m \times c \tag{2.1}$$

Where:
• c : the analyte concentration.
• y : the output signal.
• m : the sensitivity of the biosensor.

The linearity of a biosensor can be related to the resolution of the biosensor and the concentration range of the analyte being tested. Biosensor resolution is defined as the smallest change in analyte concentration required to cause a change in the biosensor response. Depending on the application, good resolution is required because most biosensor applications require not only detection of the analyte but also measurement of analyte concentrations over a wide operating range. Another term related to linearity is linear range, which is defined as the range of analyte concentrations for which the biosensor response varies linearly with concentration.

2.3.3 Sensitivity

Sensitivity shows how well a biosensor can detect small changes in refractive index. It is how much the resonance wavelength moves when the refractive index changes a little (/n). High sensitivity helps find low amounts of substances, like early signs of disease [28].

For example,figure2.14,a 2D photonic crystal biosensor with a sensitivity of 200 nm/RIU (refractive index units) can detect sub-picomolar concentrations of target molecules.

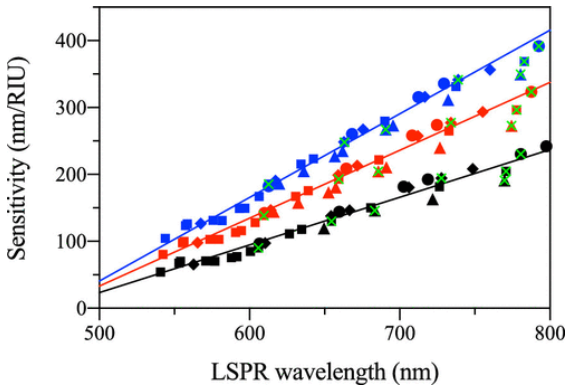

Figure 2.4: A graph showing the relationship between refractive index change and resonance wavelength shift.

2.3.4 Quality Factor (Q-Factor)

The Q-factor shows how sharp the top of the resonance is. It is the resonance wavelength divided by the width at half height of the peak. A high Q-factor means the peak is narrow. This helps the sensor tell close wavelengths apart and improves detection accuracy [29].

A 2D photonic crystal biosensor with a Q-factor of 10,000 can spot target analytes at just 1 fM levels. Figure 2.11 shows an example of quality factors for different PhC designs along with sensitivity.

$$Q = \frac{\lambda}{\Delta\lambda_{FWHM}} \tag{2.2}$$

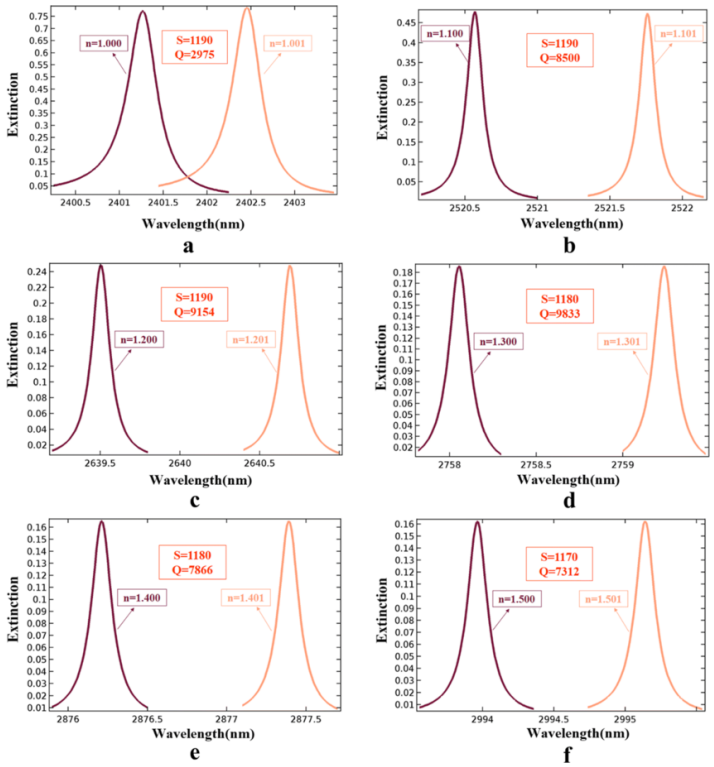

Figure 2.5: A graph comparing the Q-factor and sensitivity of different photonic crystal designs.

2.3.5 Limit of Detection (LOD)

The lowest amount a sensor can find is called the limit of detection (LOD). It depends on how good the sensor is, the noise around, and how fast molecules catch on. Making the LOD better helps in spotting tiny amounts of things, like early signs of cancer or checking the air and water. Finding small things is key for health and safety [30]. For example, Table 2.1 tackle various values of limit of detection through various applications.

$$\text{LOD} = \frac{\lambda}{10Q \times S} \tag{2.3}$$

Table 2.1: Some studies did not specify the exact LOD values.

Analyte	LOD	Reference Glucose 0.16 mM Nature Scientific Reports
Cancer Cells	0.000236 RIU	Design of Photonic Crystal Biosensors for Cancer Cell Detection
Influenza Virus	1 ng/mL	Reflectometric 2D Photonic Crystal Biosensor
Cholesterol	Not specified	Design of a Two-Dimensional Photonic Crystal Biosensor
Creatinine	Not specified	Biophotonic Sensor Based on Photonic Crystal

2.3.6 Selectivity

Selectivity is how well a sensor can pick out the right analytes from other stuff in complex samples. It's mostly set by the layer that helps the sensor work and the design of the photonic crystal framework. High selectivity as shown in Figure 2.6 is crucial for precise detection in real-world uses like medical tests and watching the environment [15].

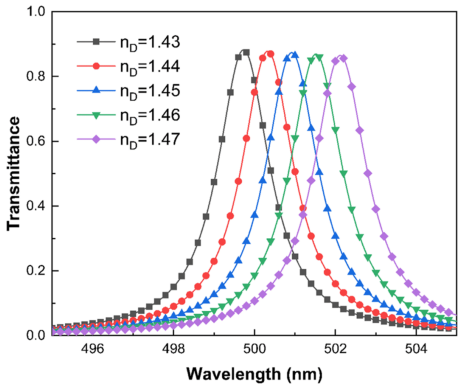

Figure 2.6: A diagram showing the selective binding of target analytes on a functionalized photonic crystal surface.

2.3.7 Response Time

Response time is how long a sensor takes to find and measure an analyte after it is exposed. Quick reaction times are key for real-time tracking and care uses. For instance, a 2D light crystal sensor with a reaction time of under 10 seconds can give fast feedback in health settings, allowing prompt decisions. The figure 2.7 illustrates that the response time.

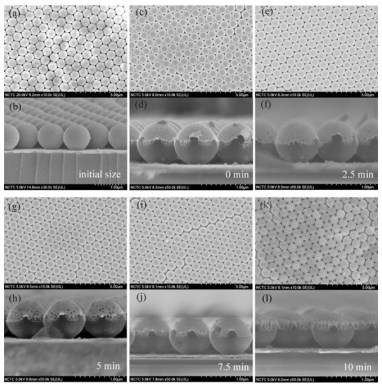

Figure 2.7: Time-Resolved Photoluminescence Decay Curve showing the intensity of photoluminescence as a function of time.

2.4 Principles of 2D Photonic Crystal-Based Biosensors

2.4.1 Photonic Bandgap Engineering in 2D PhC

Photonic crystals are tiny materials made to control light by their regular structures. A key idea is the photonic bandgap, a range where light can't go through. This gap happens because light waves interfere when they hit the regular pattern. You can change the gap by adjusting the size of the pattern, the difference in how materials bend light, and what the materials are made of. In 2D photonic crystals, the setup is a two-part grid. This grid can be square or hexagon shaped with holes in a clear material. When light hits this grid, some colors are bounced back or trapped, while others pass through. This lets 2D photonic crystals work as fine eye sensors. Any shift in the nearby light path, like when a small bit sticks to its surface, changes the gap where light can't pass and moves how light behaves. Figure 2.8 illustrates the photonic bandgap diagram for a hexagonal air-hole lattice for both TE and TM modes.

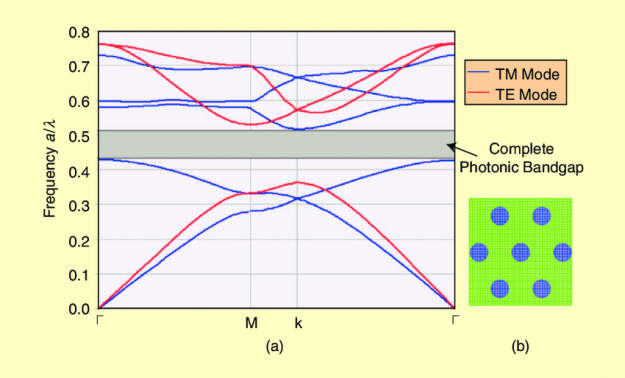

Figure 2.8: Photonic bandgap diagram for a hexagonal air-hole lattice,for both TE and TM modes.

2.4.2 Resonance Shift Mechanis

2D photonic crystal sensors measure resonance shifts. When a biomolecule, like protein or DNA, links to the crystal's surface, it changes the local refractive index. This shift moves the light's resonance wavelength in the structure. Tools like spectroscopy or imaging can see this change [27]. The change in resonance size grows with more of the analyte. This helps measure amounts of it. In a 2012 study by Lee and others, a 2D crystal device found prostate-specific antigen (PSA) with a sensitivity of 1 ng/mL.

2.4.3 Guided-Mode Resonance (GMR)

Guided-mode resonance happens when light matches with the guided modes in a 2D photonic crystal biosensor. This leads to sharp peaks that change easily with shifts in the refractive index. This boosts how much light stays inside the sensor, greatly improving sensitivity and the ratio of signal to noise [31].

The GMR biosensors work well to find tiny amounts of markers in complex samples. Figure 2.10 shows an example of resonance wavelength shift in a guided mode.

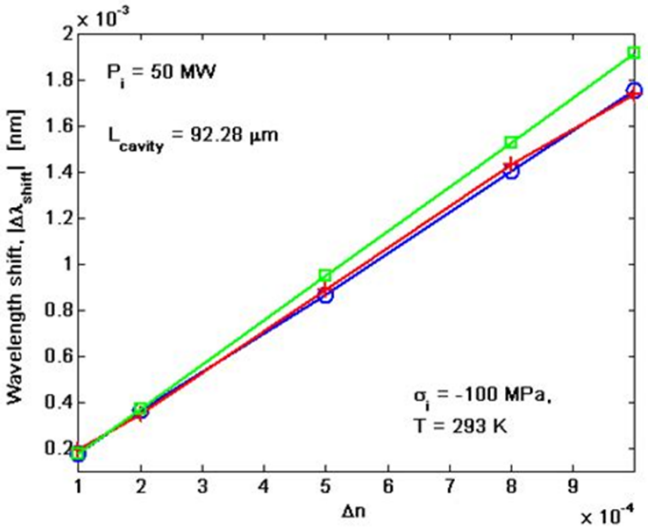

Figure 2.9: A diagram illustrating guided-mode resonance in a 2D photonic crystal.

2.4.4 Surface Functionalization

The work of 2D photonic crystal biosensors relies much on the surface treatment method. This process coats the sensor's surface with special binders like antibodies or enzymes to catch target analytes. When done well, it makes sure the sensor is precise and cuts down wrong bindings that can mess up its accuracy [32].

Ways to change surfaces include gold bits, plastic coats, and single-layer films. Gold bits can make sensors react better by changing how light bends when molecules stick. Single-layer films give a flat and steady surface to hold receptors [33].

2.5 Configurations of 2D PhC-Based Biosensors

2D light crystal sensors can come in different shapes, each made for certain uses. Choosing a shape depends on how well it can sense things, how simple it is to make, and what it needs to detect. Below, we talk about the usual shapes.:

2.5.1 Slab waveguide-based biosensors

Slab waveguides are one of the most widely used configurations for 2D PhC biosensors. Figure 2.10 represents a schematic diagram of a slab waveguide-based 2D PhC biosensor, showing light propagation and analyte binding on the surface. In this design, light is

confined within a thin dielectric slab with a periodic arrangement of air holes or dielectric rods. The presence of a target analyte (e.g., biomolecules) on the surface alters the effective refractive index, leading to a detectable shift in the resonant wavelength

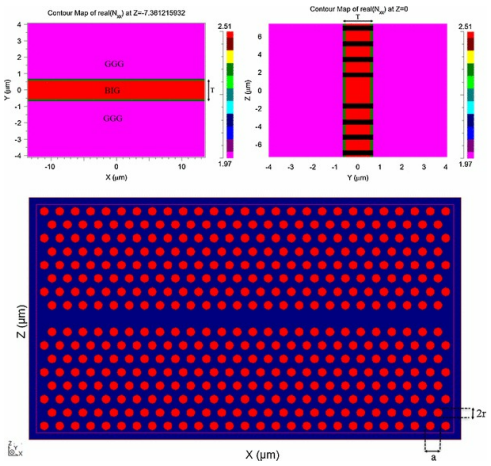

Figure 2.10: A schematic diagram of a slab waveguide-based 2D PhC biosensor, showing light propagation and analyte binding on the surface.

2.5.2 Ring resonator-based biosensors

Ring resonators are highly sensitive due to their ability to trap light in a circular path. In 2D PhC ring resonators, as shown in figure 2.11 , the resonant wavelength shifts when biomolecules bind to the ring's surface. This configuration is particularly useful for detecting low concentrations of analytes.

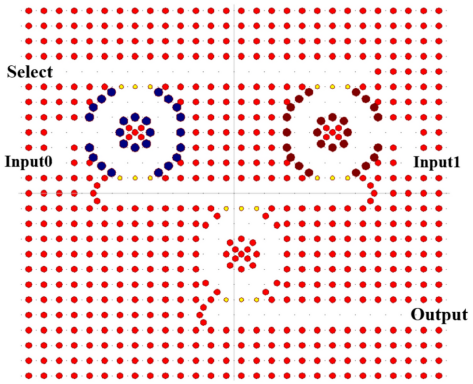

Figure 2.11: A diagram of a 2D PhC ring resonator.

2.5.3 Microcavity-based biosensors

As shown in figure 2.12, the microcavities are small defects introduced into the 2D PhC structure to localize light. When analytes bind to the cavity, the resonant wavelength shifts, providing a highly sensitive detection mechanism. Microcavities are often used for single-molecule detection.

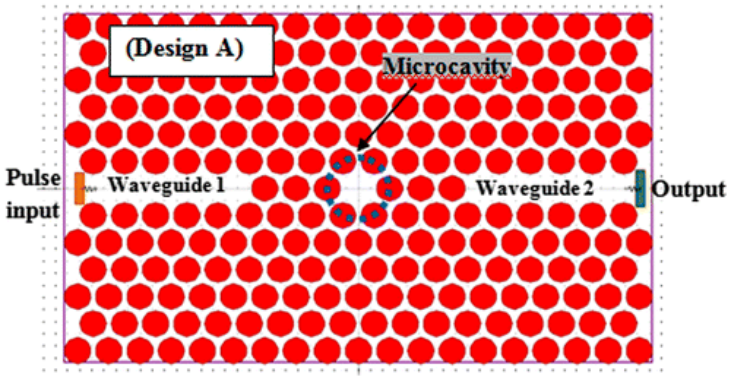

Figure 2.12: 2D PhC biosensor design based on microcavity.

2.5.4 Grating-coupled biosensors

Grating setups use a patterned surface to guide light into 2D photonic crystals. This design is great for checking samples without labels and can fit with fluid systems to watch changes as they happen.

2.6 Applications of 2D PhC biosensors

2D PhC biosensors are useful tools in many areas like disease checks and watching nature. Their strong ability to sense, easy use without labels, and chance to make small sizes make them perfect for quick tests and finding illness early.

2.6.1 Medical diagnostics

2D PhC biosensors are used a lot to find signs of illness, like cancer, diabetes, and infections (see figure 2.13). They can find cancer signs like PSA or virus proteins in blood.

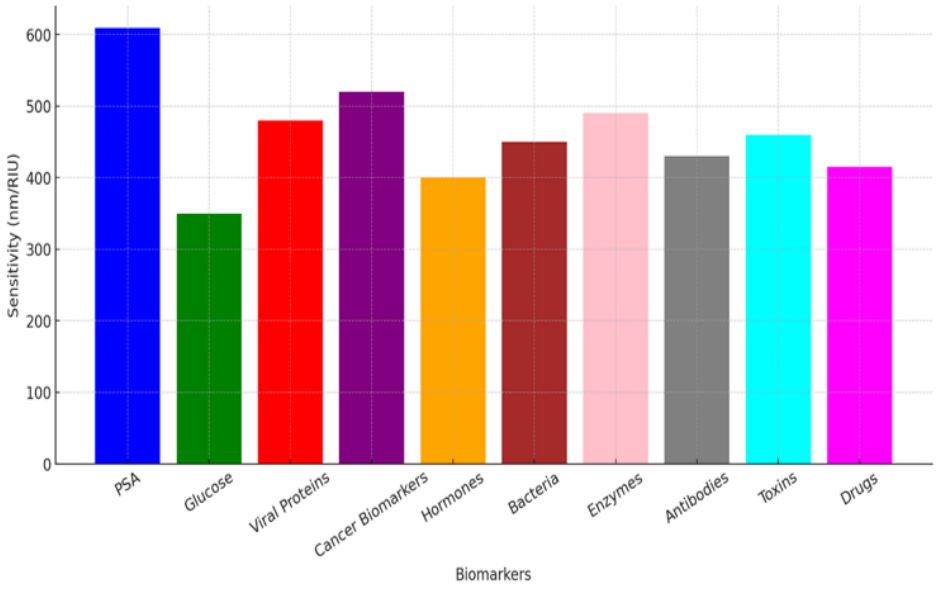

Figure 2.13: A bar chart comparing the sensitivity of 2D PhC biosensors for detecting different biomarkers.

2.6.2 Environmental monitoring

These biosensors can detect harmful pathogens or toxins in water and air, as illustrated figure 2.14.

Figure 2.14: A flowchart showing the steps involved in using a 2D PhC biosensor for environmental monitoring.

2.6.3 Food safety

2D PhC sensors find bad stuff in food, like bugs, bad chemicals, and things that make people sick. They work fast and help keep food safe to eat, table 2.2 shows different food contamination and their sensing types and Detection limit values.

Table 2.2: Food contamination and their Detection limit values.

Food Contaminant	Detection Limit	Sensor Type/Configuration
E. coli	10 CFU/mL	2D PhC with antibody functionalization
Salmonella	50 CFU/mL	2D PhC with aptamer probes
Aflatoxin B1	0.1 ng/mL	2D PhC with molecularly imprinted polymers
Pesticides (e.g., Chlorpyrifos)	0.05 ppm	2D PhC with enzyme-linked receptors
Heavy Metals (e.g., Lead)	0.01 ppb	2D PhC with chelating agents
Allergens (e.g., Peanut protein)	1 ppm	2D PhC with antigen-antibody binding

2.6.4 Drug development

In drug research, scientists use 2D PhC biosensors to look at how drugs and their targets interact. These tools help find possible drugs fast because they can test many at once and catch small changes. This speeds up finding new drugs. The figure 2.15 shows diffrent application of 2D PhC biosensors in various fields.

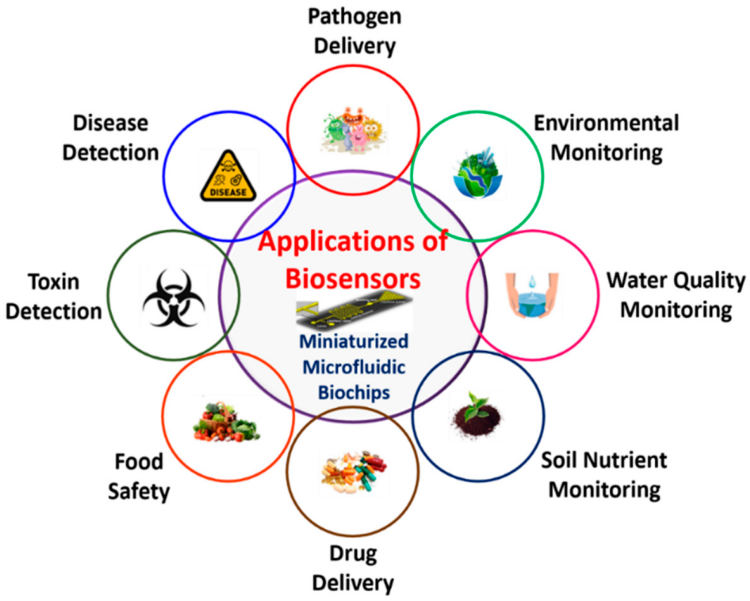

Figure 2.15: Application of biosensors.

2.7 Different diseases detectable by PhC biosensors

Photonic crystal biosensors are strong tools for spotting many illnesses. They do so because they are highly sensitive, don't need labels, and can monitor things instantly. These sensors use special light traits of photonic crystals to see biomolecule actions. This makes them good for finding infectious diseases, ongoing problems, and even gene troubles.

2.7.1 Infectious diseases

PhC sensors are good tools to find germs that make us sick. For germs like E. coli, Salmonella, and Staphylococcus aureus, these sensors have special parts that stick to germs. They can find germs with only 10 parts per mL, which helps us know if we're sick soon. For viruses like flu, HIV, or COVID-19, PhC sensors look for important parts of the virus. They give fast, true results that help in health crises. Diseases from parasites, like malaria, can be found with PhC tools too. They find key bits linked to the parasite, helping catch and treat sickness early.

2.7.2 Chronic diseases

PhC sensors are now used to check long-term health issues, needing constant and precise biomarker tracking. Cancer: PhC sensors find cancer signs like tumor cells, proteins (like PSA for prostate cancer), and DNA changes. They are very sensitive, helping spot cancer early and check how well treatments work. Diabetes: By tracking sugar levels or HbA1c, PhC sensors help manage diabetes. They offer a way to check without needing blood samples. Heart Issues: PhC sensors find signs like troponin and CRP, which help diagnose heart attacks and other heart problems quickly.

2.7.3 Genetic disorders

PhC biosensors are also capable of detecting genetic mutations and disorders: Cystic Fibrosis: By identifying specific DNA sequences associated with the disease, PhC biosensors can provide early diagnosis and facilitate personalized treatment plans. Hereditary Cancers:PhC biosensors can detect genetic mutations linked to hereditary cancers, such as BRCA1 and BRCA2 mutations, enabling proactive healthcare measures.

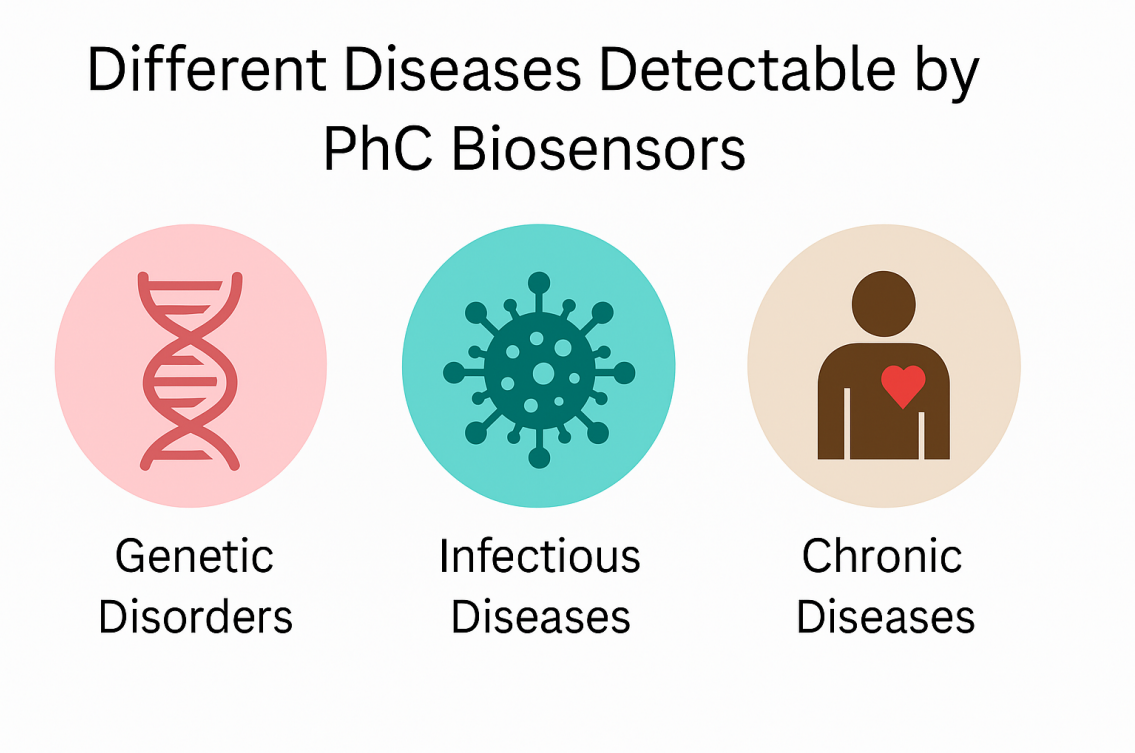

Figure 2.16: Diffrent diseases detactable by PhC biosensors

2.8 Fabrication techniques of PhC biosensors

Making photonic crystal biosensors uses top methods to craft tiny materials with exact light traits. These methods are key for making sure the biosensors are sensitive, specific, and work the same every time.

2.8.1 Top-down fabrication methods

Top-down ways make small structures by taking away stuff from bigger pieces:

Photolithography : A common way to shape tiny patterns. It uses light on a special material with a mask and then removes parts with chemicals to form the needed design.

Electron beam lithography (EBL): Lets you make very fine details, better than photolithography. It's good for making hard designs but costs more and takes longer.

Nanoimprint Lithography (NIL) : A cheaper way that presses shapes onto a surface. It works well for making many PhC sensors at once.

2.8.2 Bottom-up fabrication methods

Bottom-up ways build tiny structures from smaller bits.

Self-assembly: Uses the way molecules like to line up in neat patterns. For instance, colloidal self-assembly can form 3D photonic crystals with special light properties.

Chemical vapor deposition (CVD): This is when gas forms a solid on a surface. CVD makes top-quality photonic crystal films.

Layer-by-layer (LbL) assembly: Involves putting on layers in turns to make a photonic crystal. This lets you control how thick and what each layer is made of.

2.9 Functionalization techniques

2.9.1 Challenges in fabrication

Even with big leaps forward, lots of hurdles remain.

Scaling up: Many making methods can't be used for big runs.

Cost : High-detail ways like EBL cost a lot and need special gear.

Consistency: Getting the same good results with each batch of sensors is tough.

2.10 Conclusion

We discussed in this chapter the basic principles and advantages of biosensors based on photonic crystal (PhC) structure. Photonic crystals, due to their remarkable ability for manipulation and control of light via photonic bandgaps, offer unprecedented promise for highly sensitive, miniaturized, and label-free biosensors.
The presentation addressed the photonic bandgap formation, defect mode contribution to enhanced confinement of light, and the various mechanisms—such as resonance shift and transmission which form the basis of detection in PhC sensors.

We also talked about the role of important performance parameters such as sensitivity, quality factor, figure of merit (FOM), and detection limit (DL) and how they are related to the structural design of the photonic crystal. The emphasis was given to the use of these devices in the biomedical and environmental sectors, particularly to detect pathogens in water and biological fluids.

This introductory overview paves the way for the subsequent chapter that introduces the design and simulation of a two-dimensional photonic crystal biosensor with a ring resonator cavity. The next chapter will optimize the photonic structure for the detection of waterborne bacteria, along with an in-depth analysis of its optical response, performance parameters.

Chapter 3

Design of a 2D PhC biosensor based on a ring resonator for detecting waterborne bacteria

Contents

3.1 Introduction

Photonic crystals (PC) are modern materials that have attracted the attention of researchers due to their remarkable ability to control the propagation of light in periodic structures. This property is attributed to the formation of a photonic bandgap (PBG) [34], a range of wavelengths where light cannot propagate within the material, paving the way for a wide range of optical applications, including waveguides [18], power splitters [35–39], sensors [40], biosensors [41–43], logic gates [44]. One of the great advantages of photonic crystals is their design flexibility. By modifying the internal structure (for example, by introducing local defects), precise pathways can be created to guide and control light even in restricted areas [14]. This chapter focuses on the design and performance improvement of a 2D Photonic crystals biosensor based on a single ring resonator The intention is to optimize the sensitivity, selectivity and reduced size through numerical simulations carried out using the finite-difference time-domain (FDTD) method. This method is recognized for its accuracy in examining propagation phenomena within complex photonic devices [41].

3.2 characteristic parameters of PhC biosensors

Photonic crystal-based devices (PCs) are perceived as Photonic crystal (PC) devices are seen as one of the most effective options for managing light diffusion. This is due to their exceptional ability to trap and direct electromagnetic waves in specific areas while ensuring strong resistance to disturbances, particularly those of electromagnetic origin. The detection mechanism of biosensors utilising these structures is based on the concentration of the electromagnetic field in regions with a low refractive index, which significantly increases the device's sensitivity to subtle changes caused by the interaction of biomolecules with the detector's surface [12, 18]. Moreover, thanks to the compactness of the active detection zone, these biosensors are particularly suited for incorporation into integrated optical circuits, which simplifies their application in the medical and environmental fields. The performance of these detectors depends on the analysis of various crucial physical parameters, among which the Quality Factor is paramount. The latter is used to evaluate the accuracy and spectral selectivity of the biosensors response [15, 16]. In biosensors using photonic crystals (PCs), the primary criterion is the quality factor Q, which is used to measure the precision of the resonance and consequently, the sensor's performance in identifying subtle changes in the refractive index. The following relationship provides this factor:

$$Q = \frac{\lambda_0}{\Delta\lambda_{FWHM}} \tag{3.1}$$

where λ_0 represents the central resonance wavelength and $\Delta\lambda$. FWHM the full width at half maximum of the resonance peak. The higher the Q value, the more crucial the sensitivity and precision of the biosensor are, an essential element in the context of biomedical detection [24].

Recent research has shown that improving the quality factor allows for the development of extremely sensitive sensors, suitable for applications such as malaria detection or cancer cell detection [24].

Sensitivity is another element to consider for biosensors. Sensitivity represents the degree of variation in the signal transmitted by a biosensor following a change in the binding of an analyte to a detection rod. is represented by the expression 3.2:

$$S = \frac{\Delta\lambda}{\Delta n} \tag{3.2}$$

where $\Delta\lambda$ is the wavelength shift in the transmission spectrum. And $\Delta\ n$ is the changes in the refractive index.
Another important parameter is the detection limit, which is expressed by the following equation [19]

$$DL = \frac{\lambda_0}{10 \times S \times Q} \tag{3.3}$$

where S represents sensitivity while Q refers to the quality factor. The following parameter is the figure of merit (FOM), which is defined by the formula 3.4 [12, 45]:

$$FOM = \frac{Q \times S}{\lambda_0} \tag{3.4}$$

3.3 Design of biosensors based on a single ring resonator

Two-dimensional (2D) photonic crystals can offer a bandgap for light in all propagation directions located in the periodicity plane, thus allowing better spatial control of photons in this plane. Therefore, these structures offer greater flexibility in terms of optical confinement, which led to the choice of two-dimensional photonic crystals. This structure consists of silicon dielectric rods with a refractive index of 3.48 RIU, and they are placed in an air background with a refractive index of 1 RIU. The structure is a hexagonal lattice containing an equal number of rods in the horizontal and vertical directions, with dimensions (21 × 19) respectively. The lattice parameter of this structure is 600 nm, while the radius of the rods is 110 nm. Thus, the size of the structure is 146.2921 m^2 (see figure 3.1). We used the PWE (Plane Wave Expansion) method to analyze and determine the photonic band gaps (PBG) of the designed structure.

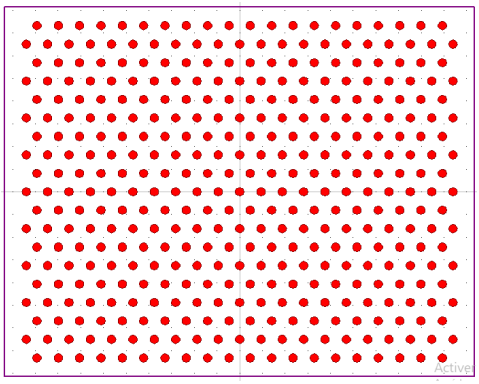

Figure 3.1: Diagram of the hexagonal lattice structure based on CPs used to design the proposed biosensor.

The table 3.1 presents the parameters of interest used in the simulation.

Table 3.1: Optical and geometric parameters of the hexagonal proposed design based on PCs.

Parameters	Values
Lattice	Hexagonal
Shape of the rods	Circles
Dimensions of the platform	(21x19 rods)
Radius of the rod (r)	110 nm
Lattice constant (a)	600 nm
Refractive index of the background (Air))	1
Refractive index of rods (Si)	3.48
Size	146.2921 μm^2

3.3.1 Calculation of the photonic bandgap (PBG)

In this part of the work, we studied the band gaps in a photonic crystal with a hexagonal periodic structure, comparing the two polarization modes: TE (Transverse Electric) and TM (Transverse Magnetic). The TE mode corresponds to a polarization where the electric field is perpendicular to the direction of propagation, while in the TM mode, it is the magnetic field that is perpendicular. The obtained results are presented in figure 3.2a, which shows how the band gaps vary as a function of the radius of the structure elements. In figure, the bands of the TE mode are represented in blue, while those of the TM mode are in red. The analysis shows that the TE mode has wider and more stable bands over a wide range of radii, while the TM mode bands are narrower and sometimes absent. This means that the studied hexagonal structure is more effective at blocking the propagation of TE waves, making this mode more suitable for applications such as optical filters and waveguides. We can therefore conclude that the TE mode offers better performance than the TM mode in this configuration. The figure 3.2b represents the band structure of a two-dimensional photonic crystal, calculated using a numerical method based on solving Maxwell's equations in periodic media. The diagram illustrates the relationship between the reduced frequency (a/ λ) and the propagation direction inside the crystal. This path allows for the representation of the variations in the properties of electromagnetic waves as they propagate in different directions within the periodic structure. The analysis considers two types of polarization: the TE mode (transverse electric field), represented by blue dots, and the TM mode (transverse magnetic field), represented by red dots. The successive dotted lines describe the band structure for each of these modes, indicating the allowed frequencies for the waves according to each crystalline direction. The areas devoid of points or lines called photonic band gaps are our particular interest, as they correspond to frequency ranges where waves cannot propagate through the material. A careful observation allows us to distinguish a well-defined photonic band gap for the TE mode between the frequencies (a/λ) 0.45 and 0.6, as well as another for the TM mode between 0.8 and 1.05. This demonstrates the ability of the studied material to block the propagation of light waves in these frequency ranges, paving the way for its use in the design of photonic devices such as optical filters or waveguides allowing precise control of light.

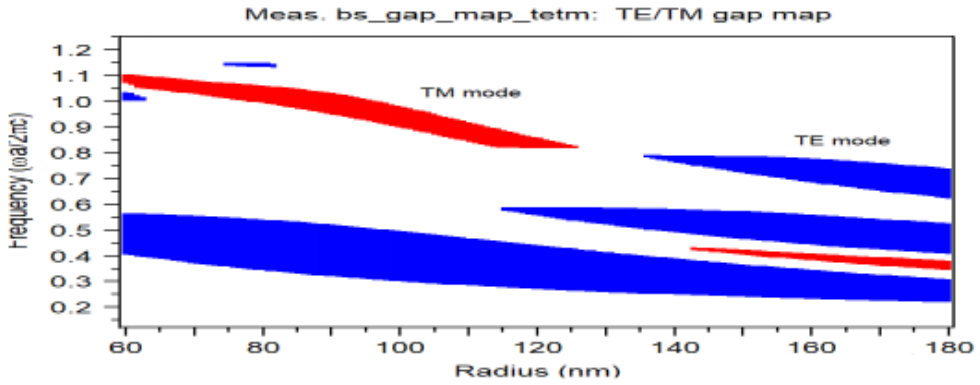

(a) Photonic band gap for TE and TM modes in a hexagonal lattice structure as a function of the rod radius.

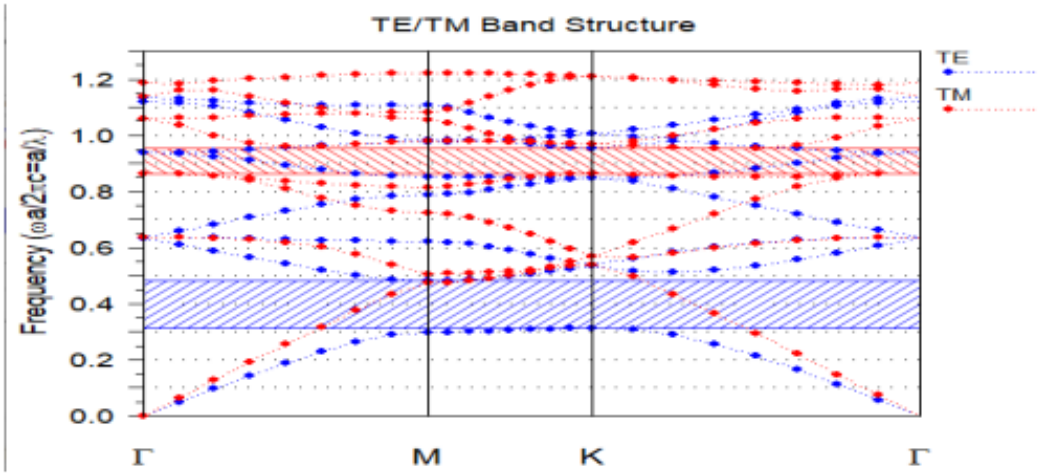

(b) Photonic bandgaps (TE) and (TM) of a hexagonal lattice structure calculated at a rod radius of 110 nm.

Figure 3.2: represents photonic bandgap in TE and TM modes

3.4 Proposed design

Our biosensor relies on the ability to detect very small variations in the refractive index. For this, we use resonant structures, whose spectral shift allows us to quantify these variations with precision. In order to optimize the sensitivity of the sensor, it is essential that this shift is as significant as possible. This drives us to design structures that maximize the interaction between light and matter, particularly at the surface, where biomolecules attach. Moreover, fine resonances are essential: the narrower they are, the more a slight spectral shift results in a clear change in intensity, which significantly improves detection.

3.4.1 Proposed structure designed with a single cavity

In this work, we have designed a photonic crystal biosensor based on a single ring resonator, as illustrated in Figure 3.3. First, we hexagonally arranged a waveguide at the

centre of a lattice of silicon (Si) rods with a refractive index of 3.48, immersed in an air medium with an index of 1. The structure is periodic with a pitch of 600 nm and a rod radius of 110 nm. Next, the cavity was formed by increasing the radius of a single rod , as illustrated in Figure 3.3. We used the plane wave expansion (PWE) method to analyse the structure, with TE polarization corresponding to the photonic crystal's band gaps. The simulation time was set to 9.134 minutes with a pulsed excitation allowing the study of the spectral response of the optical resonator.

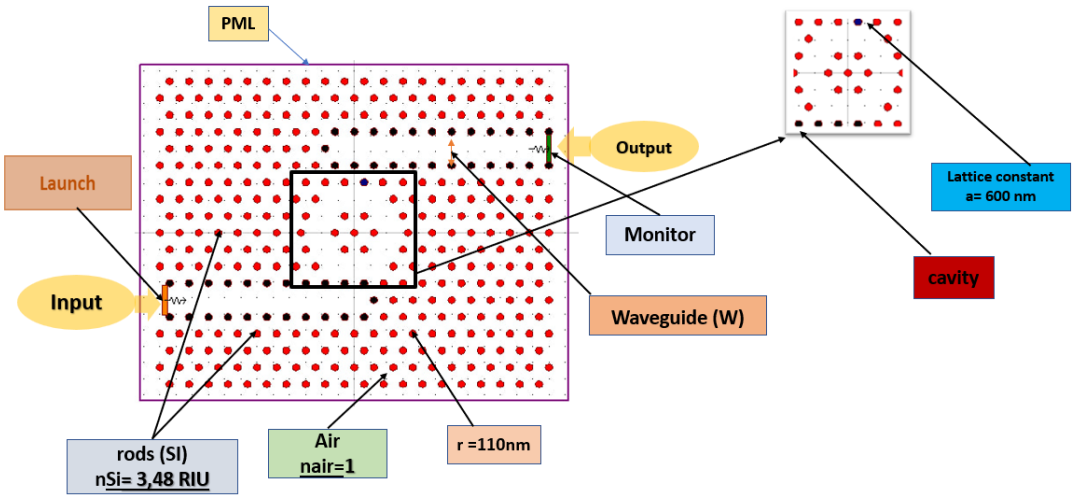

Figure 3.3: design of the proposed single-ring resonator biosensor.

3.4.2 Field distribution

Figure 3.4 shows the distribution of the TE electric field intensity generated by continuous wave (CW) excitation at a specific wavelength for the TE polarisation of the waveguide. It is observed that the light propagates only in the waveguide and in the cavity, while it is absent in the photonic crystals, which shows that these crystals act as a mirror for this wavelength, belonging to the photonic band gap. The fluctuations of the electric field are due to the fact that the light is more concentrated near the rods adjacent to the channel, where it is confined more, while it is less confined in the areas located between the rods, where it can propagate more freely.

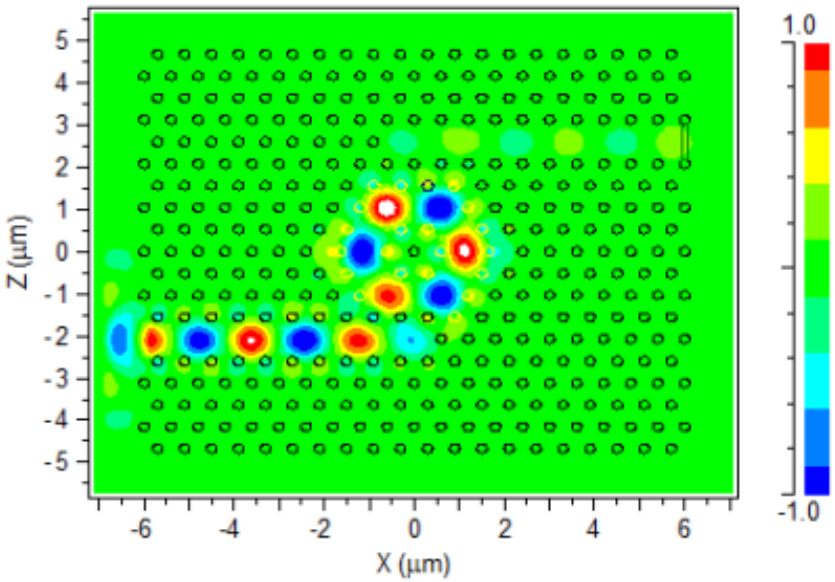

Figure 3.4: Distribution of the TE electric intensity in the cavity and the waveguide .

3.4.3 Optimization results

In order to achieve a wavelength close to 1375.7 nm, we optimised the radius of both cavity and the central waveguide rods, with the aim of designing a high-performance and highly sensitive biosensor. The radius of the rods in the structure was set to 110 nm, with a lattice constant of 600 nm. In the first step, we kept the radius of the rods located at the centre of the waveguide fixed, while varying the radius of the rods surrounding the cavity.Next, we proceeded in reverse: by fixing the cavity rods and varying those of the waveguide. In the figures below3.5,3.6 , we obtained satisfactory results in terms of resonance wavelengths and quality factors (Q).

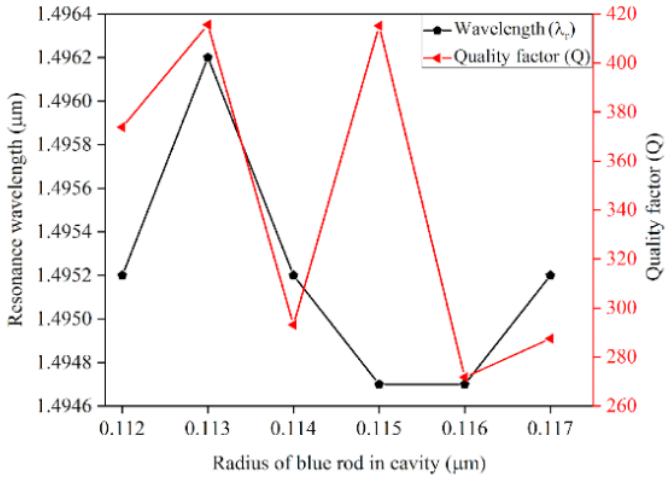

Figure 3.5: (a) shows the resonance wavelengths and quality factors as a function of the variation in the radius of the rods around the cavity,

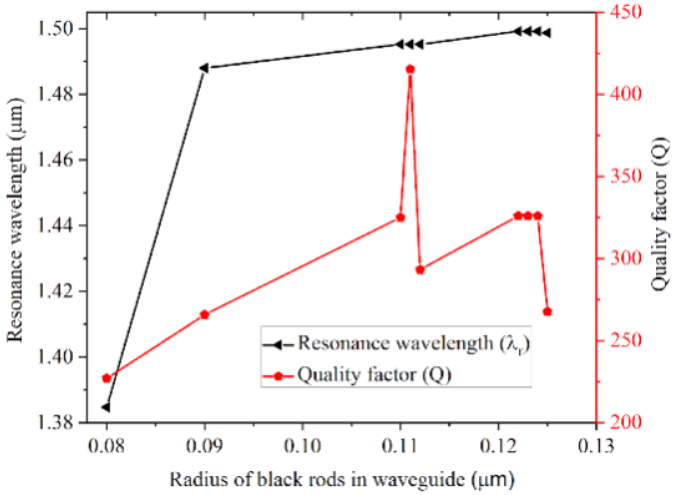

Figure 3.6: (b) illustrates the results obtained by optimizing the rods of the waveguide.

3.5 Analysis of Waterborne bacteria using the proposed 2D photonic crystal biosensor

Table 3.2: Summarizes the refractive indices of biomolecules of waterborne bacteria used in this study.

Name	RI	Source
Pure water (Reference)	1.333	[46]
V. cholera	1.365	[46]
E. coli	1.388	[46]
Cryptosporidium parvum	1.418	[47]
S. flexneri	1.422	[46]
S. flagellin	1.43	[46]
Bacillus subtilis	1.446	

The figure 3.7 presents the transmission spectra obtained at the output of the biosensor for pure water, characterised by a refractive index of 1.333. The corresponding spectrum reveals a marked resonance at the wavelength of 1375.7 nm and the Quality factor is around 598.130, with a maximum transmission rate reaching 48.77%.

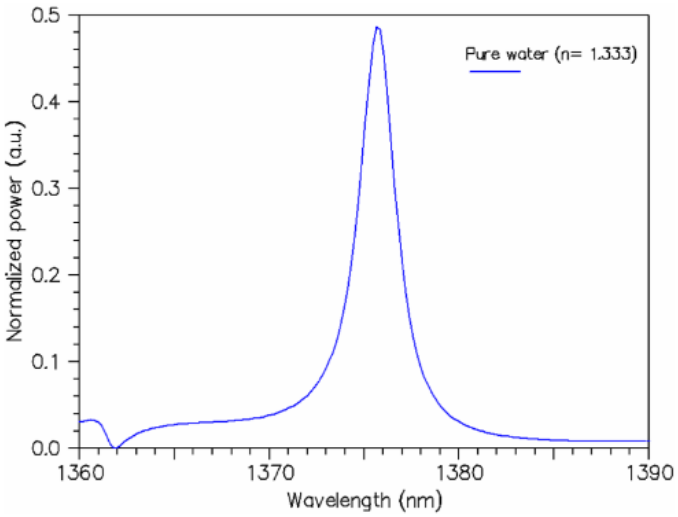

Figure 3.7: Normalized transmission power of pure water(reference).

The figure3.8 shows the transmission curve at the output of the biosensor for a single type of sample, namely V. Cholera, whose refractive index is 1.365. The transmission spectra reveal a resonance at a wavelength of 1379.9 nm and the Quality factor is around 766.611, with a transmission rate of 78.27%, which reflects the effectiveness of the biosensor in detecting this type with great precision.

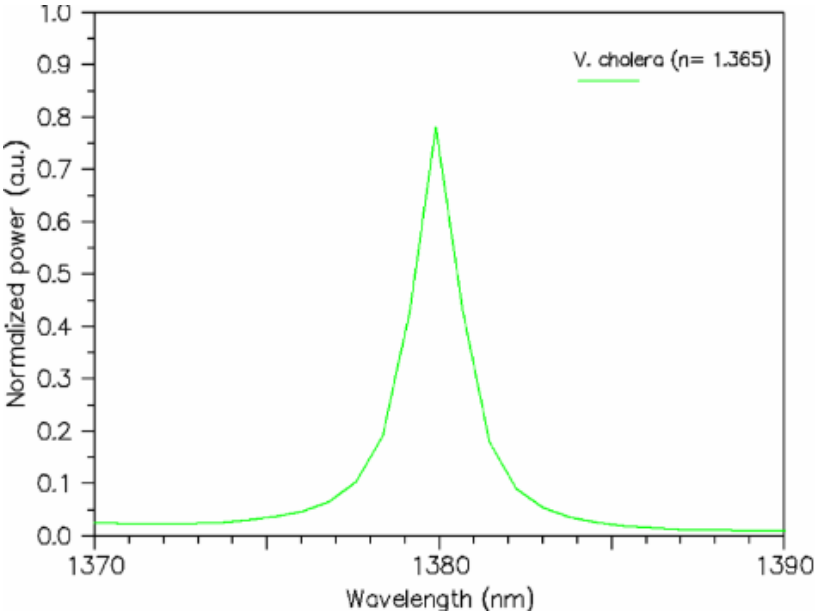

Figure 3.8: Normalized transmission power provided by the proposed PhC biosensor for detecting V.cholera bacteria.

The figure 3.9 illustrates the transmission spectrum at the output of the biosensor for the case of the bacterium Escherichia coli E. coli, whose refractive index is 1.388. The transmission spectrum reveals a resonance at a wavelength of 1383.0 nm and the Quality factor is around 864.375, with a transmission rate reaching 99.27%, which demonstrates the biosensor's ability to detect this bacterium with great precision.

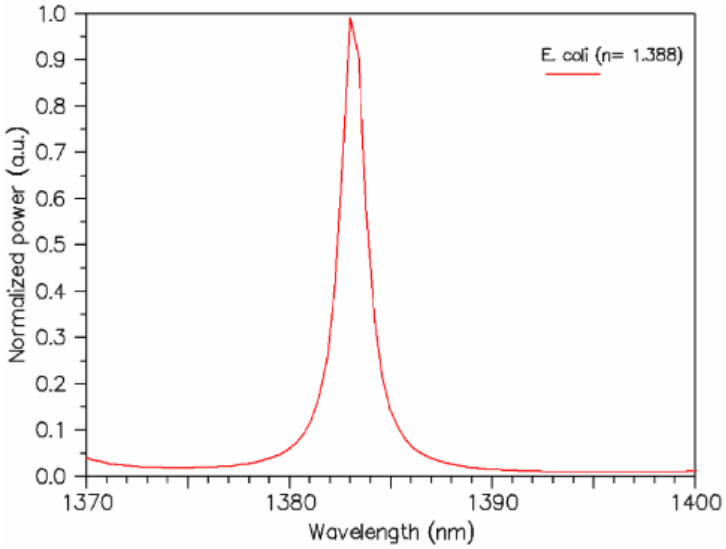

Figure 3.9: Normalized transmission power provided by the proposed PhC biosensor for detecting E.coli bacteria.

Figure 3.10 presents the transmission spectra obtained at the output of the biosensor for C. parvum, characterized by a refractive index of 1.418. The corresponding spectrum exhibits a pronounced resonance at a wavelength of 1387.1 nm, with a quality factor of approximately 433.46 and a maximum transmission rate of 70.52%.

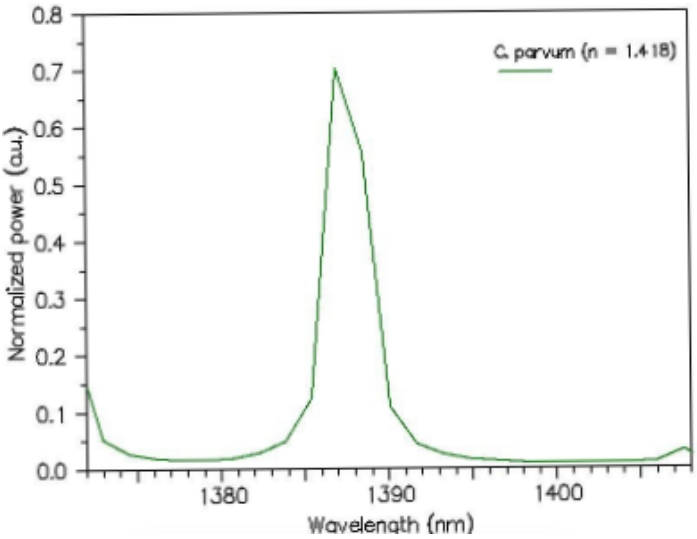

Figure 3.10: Normalized transmission power provided by the proposed PhC biosensor for detecting C. parvum.

Figure 3.11 illustrates the transmission spectrum at the output of the biosensor for the bacteria S. flexneri, whose refractive index is 1.422. The transmission spectrum reveals a resonance at a wavelength of 1388.5 nm and the Quality factor is around 694.250, with a transmission rate reaching 104.83%, which demonstrates the biosensors ability to detect this bacterium with great precision.

Note: An optical gain of approximately 0.4% was introduced into the sensor structure, which could contribute to the improvement of the transmission rate and the overall sensitivity of the device.

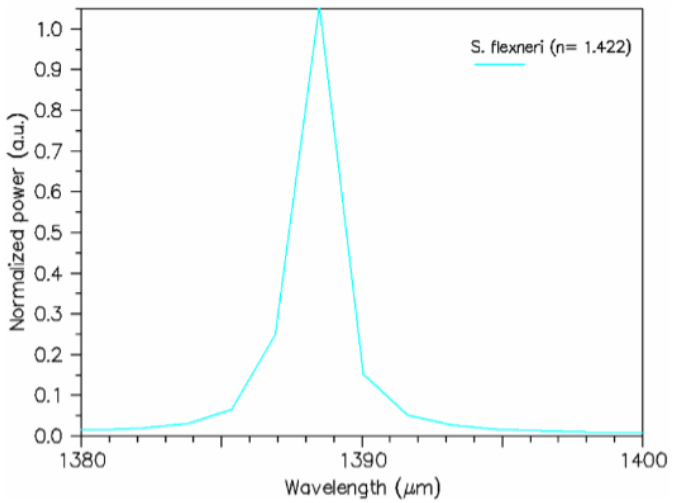

Figure 3.11: Normalized transmission power provided by the proposed PhC biosensor for detecting S.flexneri bacteria.

The figure 3.12 illustrates the transmission spectrum at the output of the biosensor for the S. flagellin bacteria, whose refractive index is 1.43. The spectrum reveals a resonance at a wavelength of 1390.1 nm and the quality factor is around 694.250, with a transmission power reaching 86.78%.

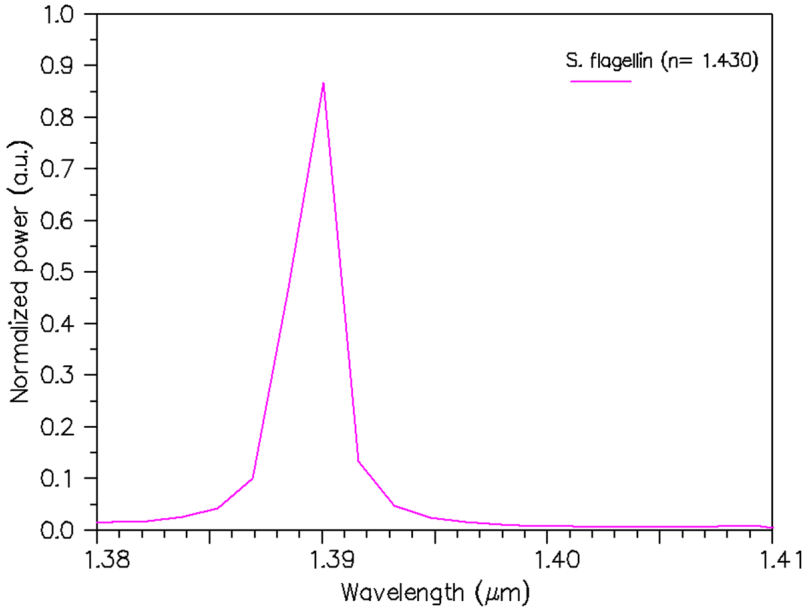

Figure 3.12: Normalized transmission power provided by the proposed PhC biosensor for detecting S. flagellin bacteria.

The figure 3.13 illustrates the transmission spectrum at the output of the biosensor for the B. subtilis bacteria, whose refractive index is 1.446. The spectrum reveals a resonance at a wavelength of 1391.7 nm and the Quality factor is around 605.09, with a transmission power reaching 97.70%.

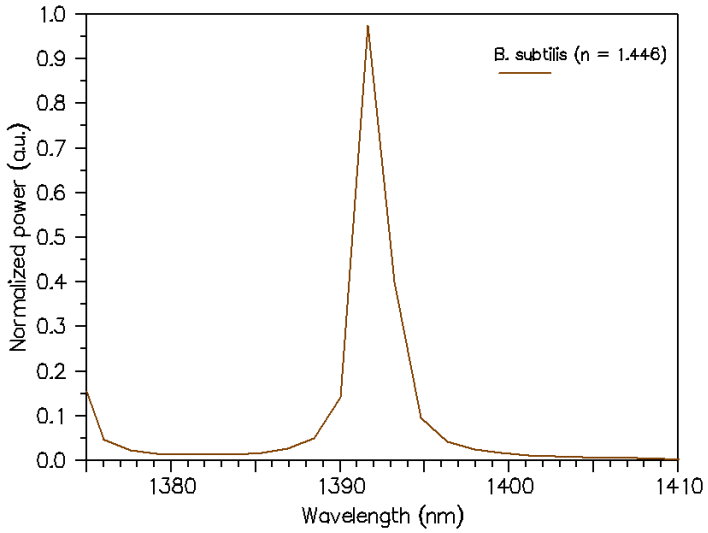

Figure 3.13: Normalized transmission power provided by the proposed PhC biosensor for detecting B. subtilis bacteria.

Figure 3.14 shows the overlay of transmission curves at the output of the biosensor for several types of bacteria present in the water. Each type is associated with a different refractive index, ranging from 1.333 to 1.430 (RIU). The table 3.3 presents the perfor-

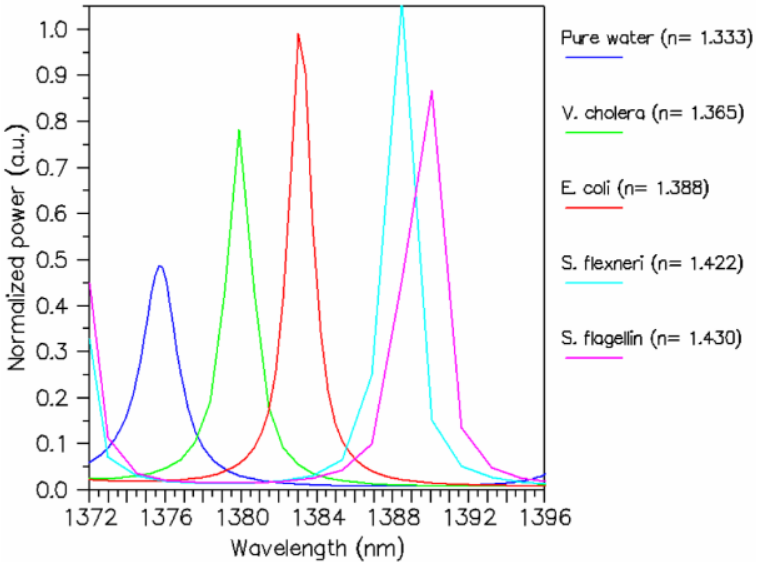

Figure 3.14: Superposition of the transmission spectra measured at the output of the biosensor for the different types of waterborne bacteria.

mance results of the biosensor in detecting different types of aquatic bacteria, where we observe the following: For E. coli bacteria, the sensor achieved the best balance among the key indicators, recording a high sensitivity of 132.73 nm/RIU, a very low detection limit of 0.00125, and a high shape factor of 82.956, reflecting an outstanding ability for precise and sensitive detection. In contrast, S. Flagellin bacteria exhibited the highest sensitivity at 148.45 nm/RIU, but it was characterized by the highest detection limit (0.00164) and the lowest shape factor (57.096), indicating that increased sensitivity does not necessarily mean improved performance, given the need for greater changes in the optical environment for accurate detection. As for V. Cholera and S. flexneri bacteria, they showed average performance between the two cases, with good sensitivity, moderate detection limits, and balanced shape factors, which emphasizes the importance of considering these indicators collectively when evaluating the sensor's efficiency in detecting various bacteria. Overall, this analysis reflects the sensor's ability to achieve sensitive and reliable detection of aquatic bacteria, provided there is an appropriate balance between sensitivity, detection limit, and FOM factor.

Table 3.3: Sensor output according to biomolecules connected to the measuring rods.

Name	RI	$\Delta\lambda_{FWHM}$	λ	Q	S	LD	FOM
Reference (Pure water)	1.333	2.3	1375.7	598.130	-	-	-
V.Cholera	1.365	1.8	1379.9	766.611	131.25	0.00137	72.917
E. coli	1.388	1.6	1383.0	864.375	132.73	0.00120	82.956
C. parvum	1.418	3.2	1386.9	433.406	131.76	0.00243	41.175
S. flexneri	1.422	2	1388.5	619.40	143.82	0.00156	71.91
S. Flagellin	1.430	2.6	1390.1	534.654	148.45	0.00175	57.096
B. subtilis	1.446	2.3	1391.7	605.9	141.59	0.00162	61.64

1.RI= Refractive index (RIU). 2.$\Delta\lambda_{FWHM}$=full width at half maximum (nm). 3. λ= Resonance wavelength (nm). 4. Q=Quality factor 5. S=Sensitivity (nm/RIU) 6. DL=Detection limit (RIU). 7. FOM=Merit factor $(RIU)^{-1}$

3.6 Linear correlation between resonant wavelengths and refractive indices

The curve shows the existence of a linear relationship between the resonant wavelength and the refractive index, where it was observed that the wavelength gradually increases with the increase in the refractive index in the range [1.333 – 1.446] RIU. This behaviour indicates that the sensor is capable of detecting small changes in its environment, particularly during variations in the concentration of biomolecules or the presence of new elements such as bacteria or proteins. The variation in resonant wavelength with respect to the refractive index is given in the following linear regression equation based on simulated data:

$$\lambda = 144.38 \times n + 1182.94 \tag{3.5}$$

The value of the coefficient ($R^2 = 0.993$) of determination confirms that the data follow a linear curve with great precision, reflecting the reliability of the system and its consistent response. The slope of the line (144.38 nm/RIU) shows that the sensor has good sensitivity, allowing it to detect small variations in the refractive index and convert them into measurable and analyzable signals. This type of relationship is very useful in biosensing applications, where the sensor can be used to detect the presence of microscopic organisms such as aquatic bacteria, as their presence modifies the refractive index and thus causes a clear shift in the resonant wavelength.

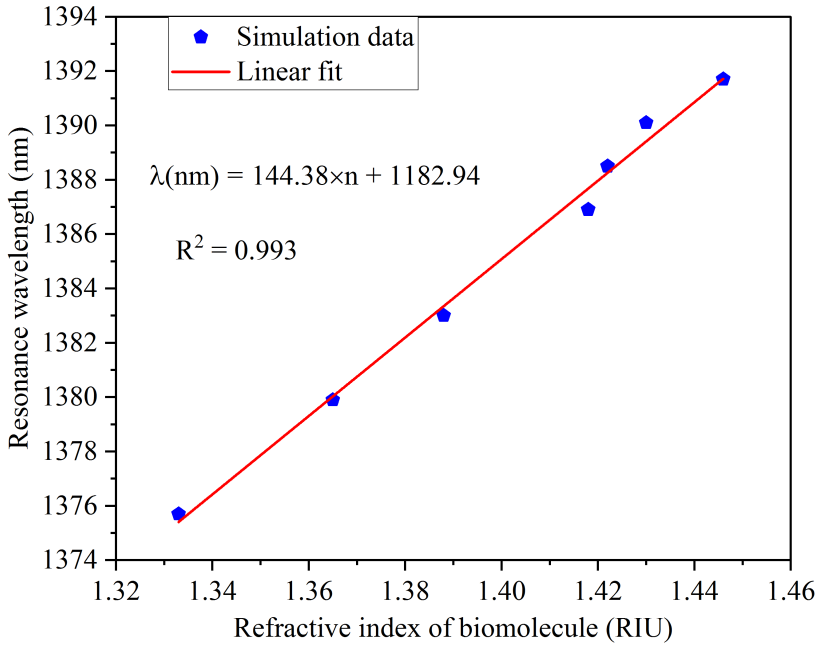

Figure 3.15: correlation between resonance wavelength and the refractive indices of different bacteria.

3.7 Conclusion

In this work, we designed and analyzed a biosensor based on a two-dimensional photonic crystal structure integrating a single cavity. The objective of this sensor is to accurately detect waterborne bacteria by monitoring the variations in the transmission spectrum related to changes in the refractive index. The simulation results showed that the sensor exhibits good optical performance, with high quality factor values and appreciable sensitivity, in addition to a clear ability to differentiate between different bacterial strains. These characteristics make it a promising tool for environmental monitoring and early detection of biological contaminants.

Chapter 4

Design of 2D-PhC biosensor based on a dual-ring resonator for high precision detection of waterborne bacteria

Contents

4.1 Introduction

Biosensor designs comprising a waveguide coupled with two cavities, commonly referred to as dual-cavity photonic crystal structures (PhC), are an emerging type of optical sensing device. They incorporate two similar resonant cavities within a two-dimensional photonic crystal lattice. The size and shape of the cavities can differ depending on the design requirements. The cavities are purposely designed to have strong optical confinement and selective resonance with specific wavelengths of light.

These dual-ring resonator systems are promising at sensing and analyzing a diverse array of biological analytes, ranging from proteins and nucleic acids to viruses and bacteria and even entire cellular structures. They are so effective that they have emerged as indispensable tools in a wide range of fields such as biomedical research, clinical diagnostics, disease monitoring, food quality, and environmental surveillance.In our study, we worked on the presence of the viruses and bacteria in contaminated water.

Here in this chapter, we focused on the devloppement of a new design of 2D photonic crystal biosensors based on a dual-ring resonator and enhancement of its performance . We begin by presenting the proposed design , including the type of lattice, material, and cavity design,ect. This is followed by the optimization of the raduis of rods of both waveguide and cavities for target specifications in resonance wavelength and quality factor (Q). We then carry out simulations results to evaluate sensor detection performance .

Exploiting the advantages of dual-ring resonator and strong localization default of photonic crystals, the design should significantly enhance sensitivity and selectivity for label-free waterborne bacteria and other microagent detection.

4.2 Proposed design

4.2.1 Structure with waveguide coupled to dual ring resonator

In order to design the proposed photonic crystal biosensor architecture, we used a two-dimensional (2D) PhC square lattice of dielectric rods in air. The entire structure consists of 33×31 dielectric rods with a lattice constant of 600 nm and an average rod radius of 110 nm. The rods are composed of silicon (Si) with a refractive index of 3.48 and a background air with refractive index 1.0. the proposed 2D PhC biosensor designed with two ring resonators is presented in Figure 4.1. as shown in Figure 4.1, the proposed biosensor is formed from input and output horizantal waveguide and two serie sumilar circular cavities. The most important functional part of the biosensor is a horizontal waveguide formed when a complete row of rods is cut along the horizontal centerline of the crystal. This line-defect waveguide is used for light propagation and can be seen in the figure as a series of smaller blue rods, which are buffer rods to make changes to the propagation and coupling efficiency. These waveguide rods passed through an optimization process.

Two circular ring resonators are vertically placed, symmetrically at the structure center with an input waveguide under the cavities and an output waveguide above the cavities. These form the dual-cavity system. Two cavities are formed by locally altering a number of rods in a ring pattern, effectively producing a ring resonator-type defect. the raduis of the bleu , yellow and black of the proposed structure will be optimized in the next section of our work in order to enhance the quality factor. The rings are formed by rods of different radius (yellow in the figure) and a missing central rod, providing strong confinement of light in each resonant loop. The cavity radius is approximately 121 nm,

slightly greater than the waveguide rods to ensure resonant coupling.

These two cavities are side-coupled to the center waveguide, enabling evanescent field coupling. Such a configuration enables strong light-matter interaction—desirable in biosensing applications such as the sensing of biomolecules or bacterial analytes.

The input and output ports are placed along the left and right boundaries of the waveguide, respectively. The structure supports Transverse Electric (TE) polarization, and its response in the form of spectra is studied using the Finite-Difference Time-Domain (FDTD) approach. For bandgap calculations, the Plane Wave Expansion (PWE) approach is used. The 653 minutes simulation runtime is used, with a broadband pulsed excitation source to observe spectral transmission and resonance shifts due to the presence of analytes. This dual-ring resonator structure enhances the biosensor's sensitivity, quality factor (Q), and wavelength selectivity, which is a highly effective structure for label-free, real-time biological sensing.

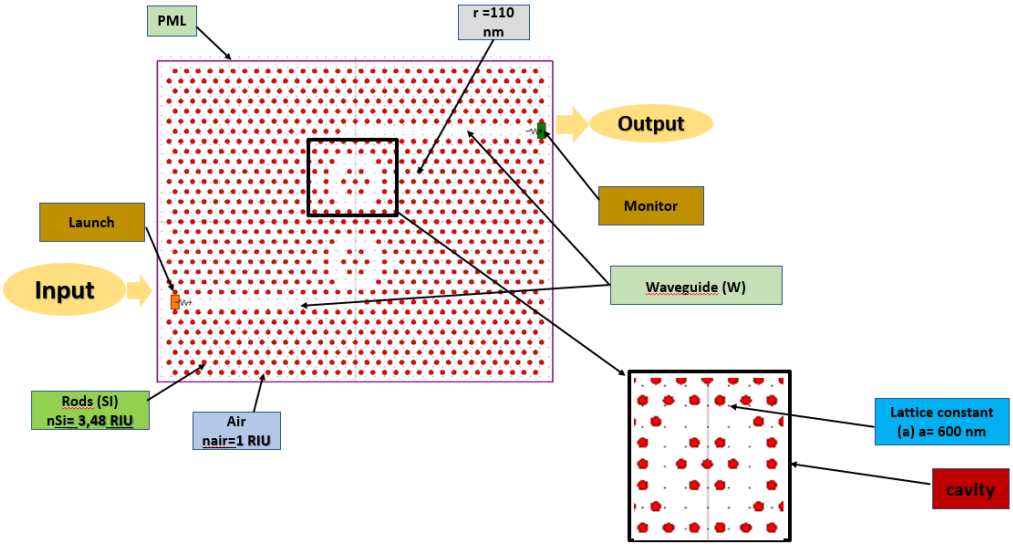

Figure 4.1: Proposed 2D photonic crystal (PhC) biosensor designed with two ring resonators.

4.2.2 Optimization of the 2D photonic crystal-Based biosensor structure

In order to achieve a resonance wavelength close to 1550 nm—which corresponds to the third optical telecommunication window—and to develop a high-quality and highly sensitive biosensor, we performed optimization on key structural parameters. Specifically, we adjusted the radii of the rods surrounding the cavity and the radius of the rods forming the waveguide (W). Figure 4.2(a) illustrates the variation of resonance wavelengths and quality factors as a function of the radius of the rods surrounding the cavity. Likewise, Figure 4.2(b) shows how the resonance wavelengths and quality factors change with variations in the radius of the waveguide rods. This parametric optimization allows for the fine-tuning of the biosensor's spectral response and enhances its ability to detect slight changes in the refractive index of the target analyte, contributing to better sensitivity and performance.

To achieve a high-performing biosensor—i.e., one with high sensitivity, a good quality factor (Q-factor), and a resonance wavelength in the vicinity of 1550 nm (third optical telecommunication window)—we performed a three-stage optimization process. This involved the adjustment of geometrical parameters of specific groups of rods within the photonic crystal structure, as illustrated in Figure 4.1.

4.2.2.1 Phase 1: Optimization of the Yellow Cavity Rods

In phase 1, the radius of the yellow rods forming the dual-ring cavity was optimized. These rods have a significant influence on the light confinement and resonant properties of the biosensor.

The objective in this phase was to maximize the Q-factor and tune the resonance wavelength close to 1550 nm by varying the radii of the cavity rods. A parametric sweep was conducted to analyze the impact of these variations. As a result, the optimal radius was found to be 121nm with a resonance wavelength of 1400nm, and Q-factor of 1364. Figure 4.2 presents the optimazation process of the radius with their corresponding Q-factor value.

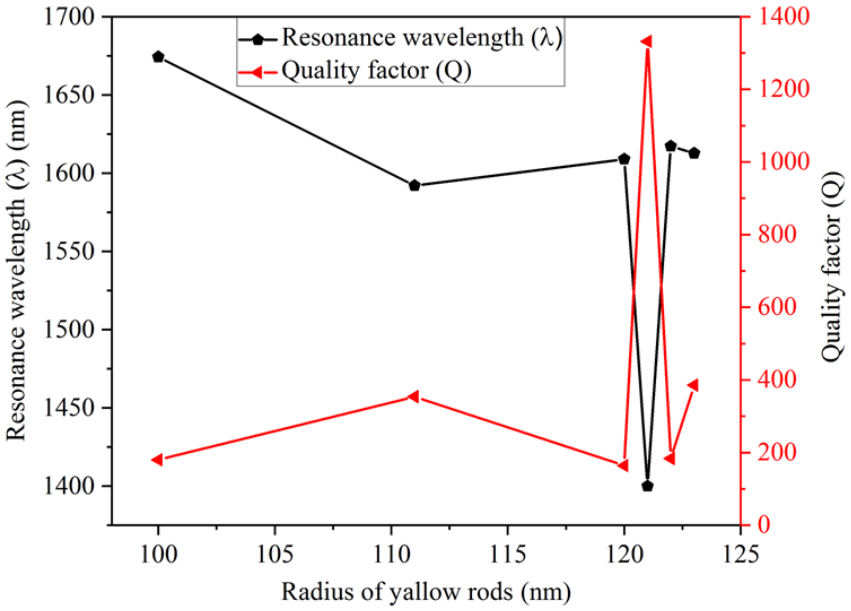

Figure 4.2: optimization of the yellow rods radius with their corresponding Q-factor

4.2.2.2 Phase 2: Optimization of the black coupling Rods

The second phase focused on the black rods in the coupling region between the cavity and the waveguide. These rods play a subtle but important role in controlling coupling strength and minimizing field leakage.

This phase aimed to enhance light confinement and the efficiency of energy transfer from waveguide to cavity by adjusting the radius of the black rods. Through systematic variation, we achieved improved spectral stability and minimized transmission loss. The optimal radius was found to be 110 nm, corresponding to a resonance wavelength of 1487.8 nm, a Q-factor of 330.79. Figure 4.3 presents the optimization process of the radius with their corresponding Q-factor value

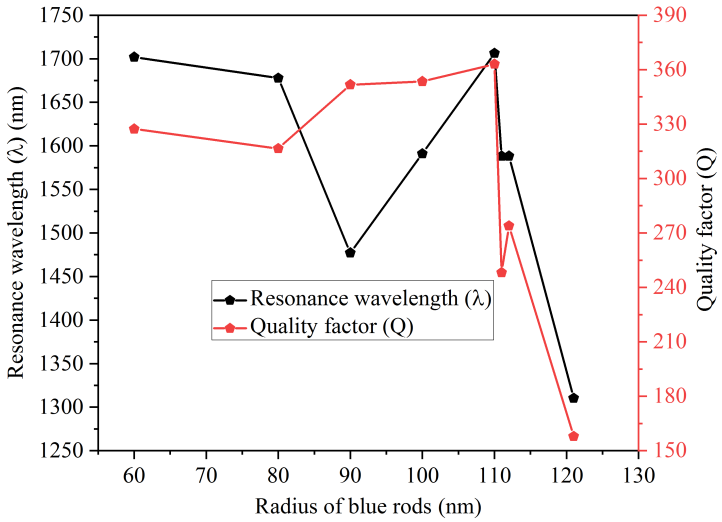

Figure 4.3: optimization of the black waveguide rods radius with their corresponding Q-factor.

4.2.2.3 Phase 3: Optimization of the blue waveguide rods

The third and final phase concerned the blue rods that form the waveguide channel. These rods are essential for guiding light and ensuring proper mode coupling into the dual-ring cavity.

This phase aimed to optimize the blue waveguide rods so they efficiently direct light and enhance coupling into the cavity. By adjusting their radius, we refined the transmission spectrum and increased field localization. The optimal radius found was 123 nm , with a resonance wavelength of 1310.2, a Q-factor of 157.85. Figure 4.4 presents the optimization process of the radius with their corresponding Q-factor value.

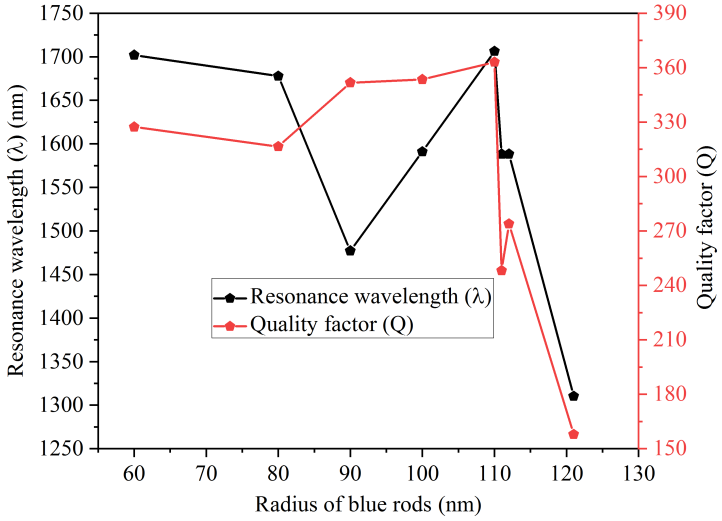

Figure 4.4: optimazation of the blue rods raduis with their corresponding Q-factor.

Table 4.1: final optimized Optical and geometric parameters of the hexagonal structure based on PCs.

Parameters	Values
Lattice	Hexagonal
Shape of the rods	Circles
Dimensions of the platform	(31x33 rods)
Radius of the rod (r)	110 nm
Lattice constant (a)	600 nm
Refractive index of the background (Air))	1 RIU
Refractive index of rods (Si)	3.48 RIU
Radius of the waveguide rods	123 nm
Radius of the cavity rods	121 nm
Radius of the black coupling rods	110 nm
Size	349.7 μm^2

The figure4.5 represents the final optimized design by enhancing the radius of the cavity , the wavelength and the black coupling rods.

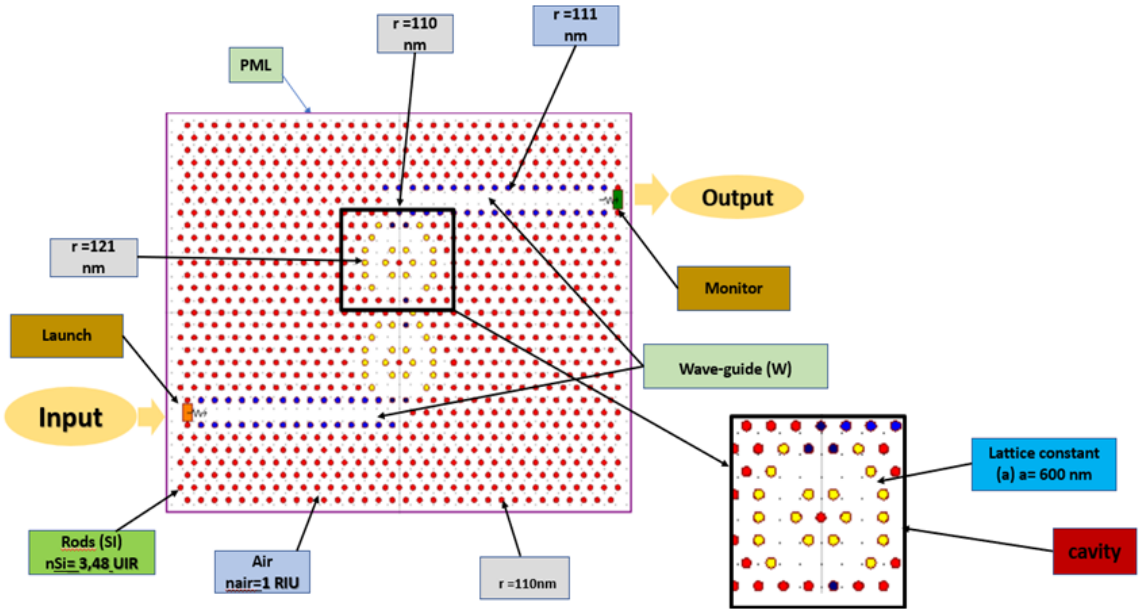

Figure 4.5: Final optimized proposed design.

4.2.3 Field distribution and transmission signal

Figure 4.6a depicts the electric field intensity variation under CW illumination at wavelength 1516.3 nm for the TE mode of the two-cavity waveguide. The figure confirms that this wavelength lies in the photonic bandgap region for which the crystal acts as a mirror. The introduction of the defects therefore leads to the guided and confined light to generate an optical guidance effect. It can be observed that the light only propagates within the waveguide and the two coupled cavities but not in the photonic crystals. It can easily be observed from this figure that the electromagnetic wave is well confined within the

structure. The oscillation of the electric field takes place due to higher confinement at the adjacent rods of the channel and lower confinement in the inter rod regions.

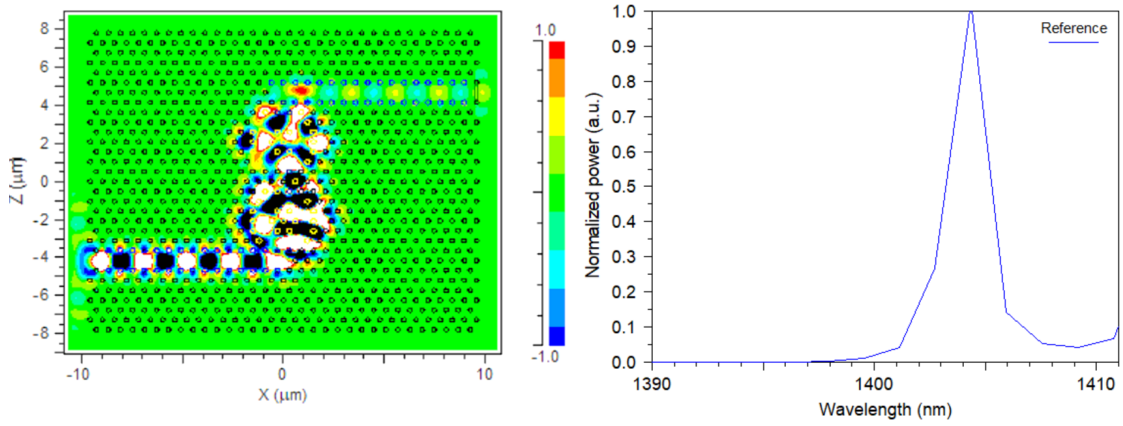

(a) (b)

Figure 4.6: (a) Distribution of the TE electric field intensity.
(b)The transmission spectrum at a wavelength of 1404.5 nm and a transmission power of 100%.

4.3 Selection of the biomolecules rods

The selection of biomolecules for a given application in a 2D photonic crystal biosensor, with a coupled waveguide and two cavities, depends upon the thoughtful balancing of a series of key criteria.These include the nature of the target analytes, the interaction specificity and affinity, the stability, sensitivity, and availability of the biomolecules". Sensitivity and detection limit of the biosensor are also crucial: we select biomolecules in such a manner that sensitivity is adequate for quantitation of target analytes in the application conditions. We then confirm that the biosensor detection limit is consistent with the concentrations of analytes that are expected to be present in the sample. We placed the biomolecules in the green rods surrounding the two cavities in this work, since they have a very good location within regions of high concentration of the electric field. These positions are particularly ideal for sensing, as small changes in refractive index due to molecular interactions directly impact the resonant properties of the structure. The optimization procedure included simulating the photonic response with incremental introduction and placement of the green rods. We tracked how the spectral response and quality factor varied in each setup. The distribution we used allowed us to optimize sensitivity as well as specificity. By locating the biomolecules in the center of the sensing region—at the two cavities—our placement allowed us to maximize the interaction of light with the biological material to be as intense and localized as possible. This produces a very large resonant wavelength shift upon analyte binding, with minimal interference from other components in the structure.

In the first structure(a), the biomolecule is introduced only around the cavity (green rods)with the number of biomelecule is N=2, whereas in the second structure(b), the biomolecule fills both the center and the entire cavity region with the number of biomelecule is N=12. a resonance peak was observed at 1363.9 and 1399.5 nm respecitvely, with transmission powers measured at 50% and 42% respectively and for the quality factor 1363.9 and 1166.25, respectively.

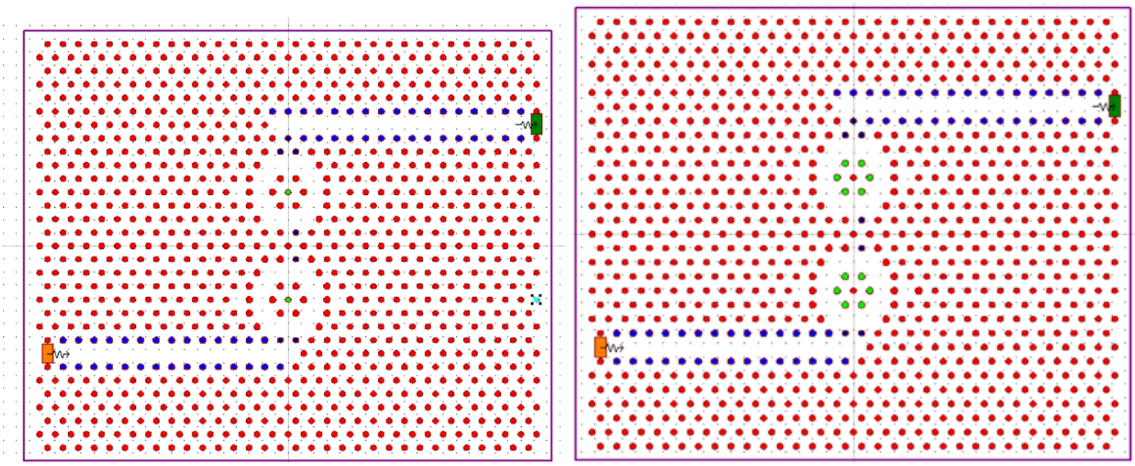

(a) (b)

Figure 4.7: (a) The proposed PhC biosensor connected with two biomelecule rods (N= 2). (b) The proposed PhC biosensor connected with two biomelecule rods (N= 12).

In the first structure(a), the biomolecule is introduced only at the center of the cavity (green rods), whereas in the second structure (b), the biomolecule fills both the center and the entire cavity region and beside the cavity In the case of the first configuration (center-only placement), a resonance peak was observed at 1399.5 and 1414.5 respectively, with transmission powers measured at 47% and 87% respectively and for the Quality factor 1272.27 and 1767.5 respectively. making the structure 4.8 with N=36 a perfect choice of biomolecules placement, the resonance shift became more pronounced, indicating stronger interaction between the light field and the biomolecule. This led to enhanced quality factor and power.

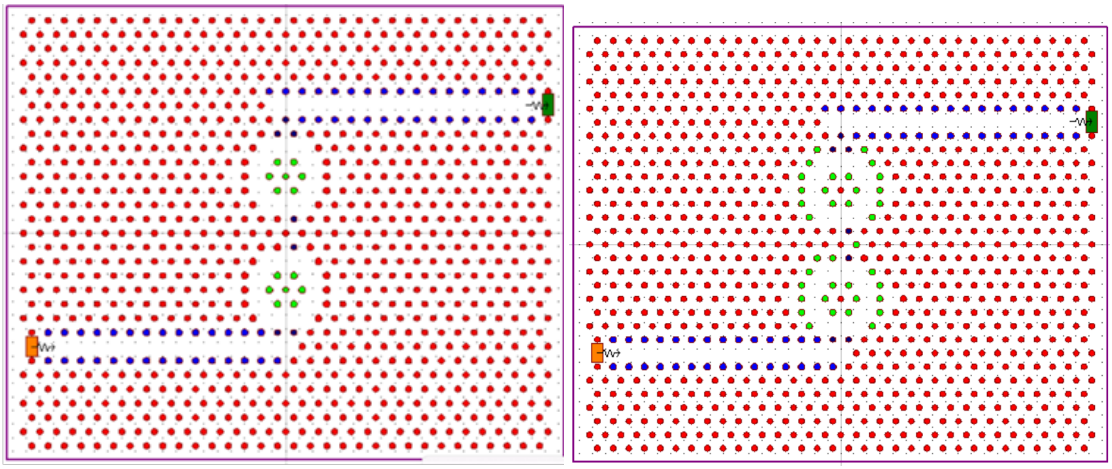

(a) (b)

Figure 4.8: (a) The proposed PhC biosensor connected with two biomelecule rods (N= 14). (b) The proposed PhC biosensor connected with two biomelecule rods (N= 36).

In this structure, the biomolecule is introduced the biomolecule fills the entire cavity region except the center. a resonance peak was observed at 1363.9 nm with transmission power measured at 47% and the Quality factor 1272.27.

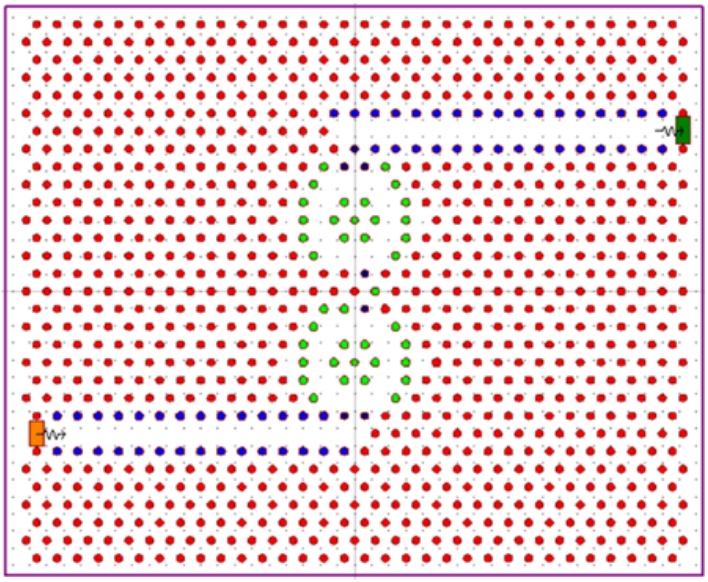

Figure 4.9: The proposed PhC biosensor connected with two biomelecule rods (N= 38)

4.4 Analysis of waterborne bacteria detection using the proposed 2D PhC biosensor

Waterborne diseases are a serious public health concern for both human and animal populations. Pathogenic microorganisms (primarily bacteria, protozoa and viruses) responsible for waterborne disease are capable of causing large-scale epidemics with significant environmental effects. Contaminated water supplies are major vectors of these pathogens making it an important global water quality threat. Common examples of waterborne bacteria include Vibrio cholerae, Salmonella typhi, and Escherichia coli (E. coli) that contribute largely to microbial pollution in aquatic systems. Reports of human infections typically include symptoms such as nausea, vomiting, abdominal cramps, and diarrhea [1]. A reported case in Canada identified E. coli contamination that contributed to the deaths of 7 people and total of over 2300 reported infections in 2000 [2]. This study presents new environmental and health uses, in which the biosensor's speed, sensitivity, and linearity are critical to the early detection and monitoring of waterborne diseases. Here , we performed the detection of two major bacterial contaminants found in water along with air, which served as a reference mode. Detection was realized owing to the particular binding of target pathogens to the biomolecule-coated rods in the two resonant cavities of the photonic crystal. FDTD technique was used to acquire the simulation results.

Figure 4.10 indicates the transmission spectrum at the biosensor output upon detecting pure water, with a refractive index of 1.333. Examination of the transmission in pure water has a well-defined resonant wavelength of 1404.4 nm quality factor of 702.20 and the measured transmission power of 100%.

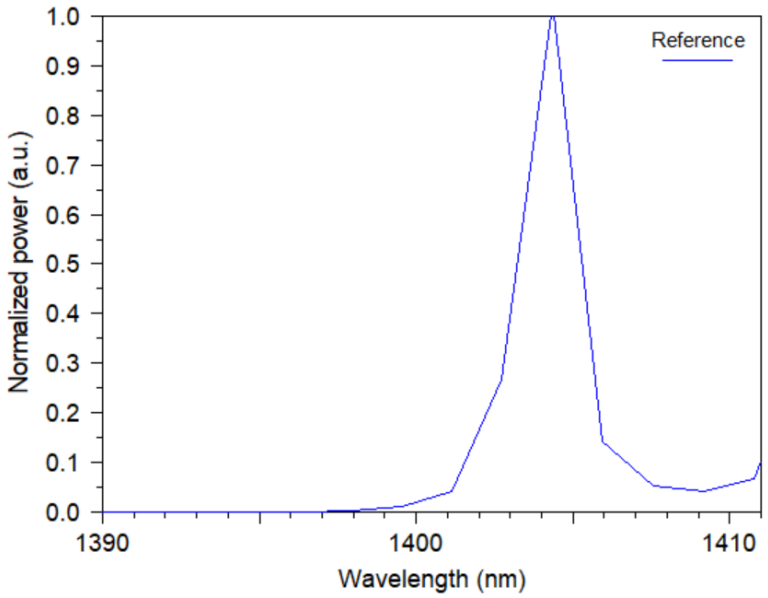

Figure 4.10: Normalized power of the biosensor reference (Pure water).

Figure 4.11 shows the normalized transmission spectrum by the proposed biosensor for the detection of Vibrio cholerae biomolecule with a refractive index of approximately 1.365. The resonant wavelength (λ) and quality factor (Q) are 1408.3 nm and 1083.3, respectively. The measured transmission power is 75%.

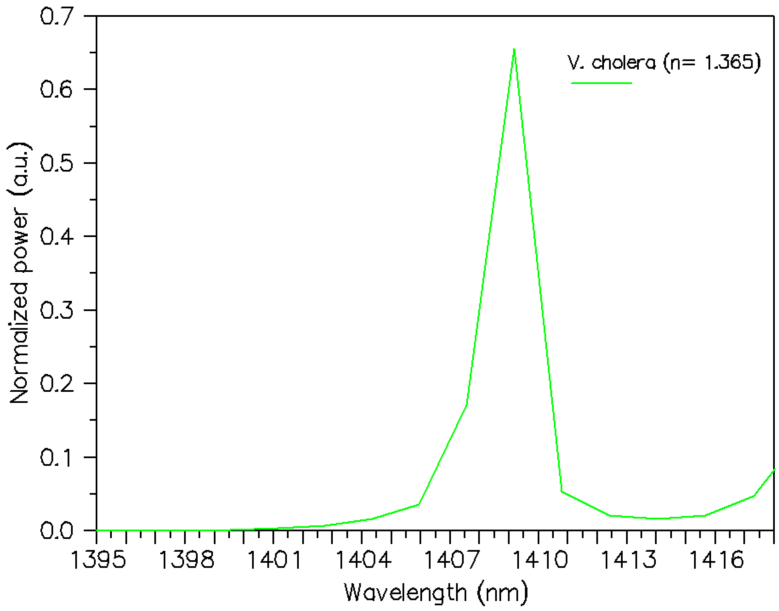

Figure 4.11: Normalized power of the biosensor for Vibrio cholerae.

Figure 4.12 shows the transmission spectrum at the output of the biosensor for the detection of Escherichia coli with refractive index of approximately 1.388. The resonant wavelength (λ) and quality factor (Q) are 1412.5 nm and 1569.4, respectively. The measured transmission power is 87.58%.

Figure 4.13 illustrates the transmission spectra at the biosensor output for the Cryptosporidium parvum bacteria with the refractive index of 1.418. The transmission measurements resonance was at the wavelength of 1416.5 nm and The measured transmission

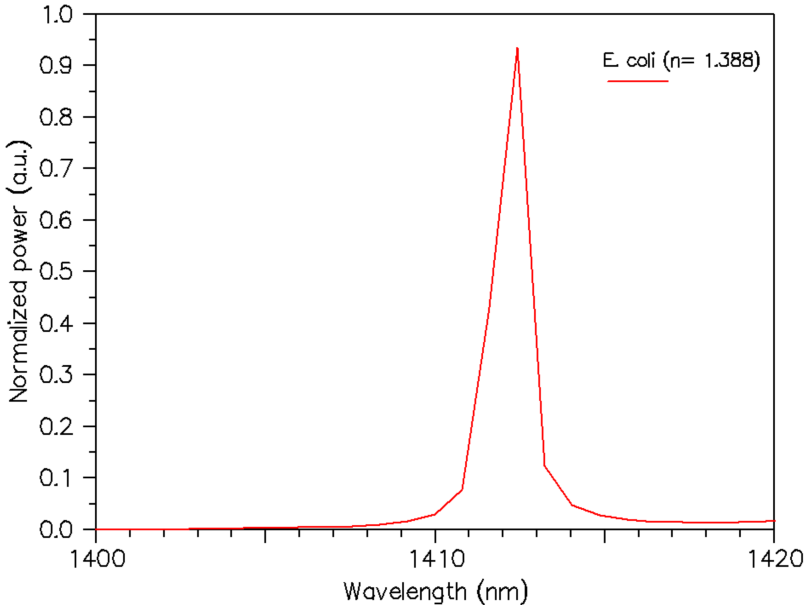

Figure 4.12: Normalized power of the biosensor for Escherichia coli.

power is 75%.

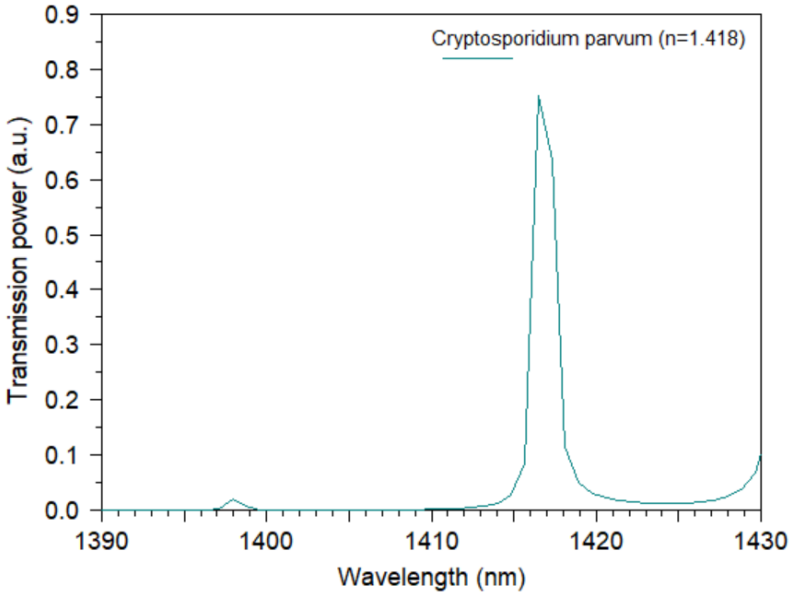

Figure 4.13: Normalized power of biosensor for cryptosporidium parvum.

Figure 4.14 illustrates the transmission spectra at the biosensor output for the Shigella flexneri bacteria with the refractive index of 1.422. The transmission measurements resonance was at the wavelength of 1497.3 nm and The measured transmission power is 63%.

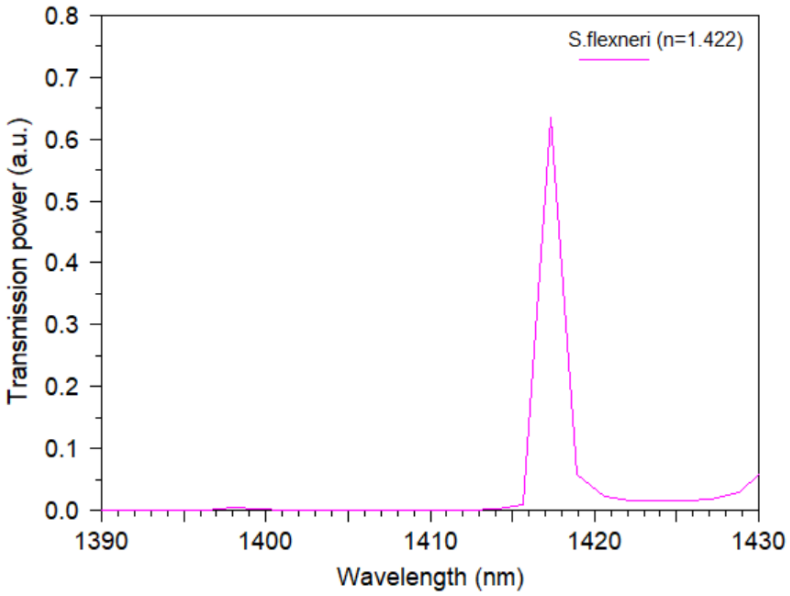

Figure 4.14: Normalized power of biosensor for Shigella flexneri.

Figure 4.15 illustrates the transmission spectra at the biosensor output for S.flexneri, with refractive index of 1.43 RIU. The resonance wavelength of 1497.3 nm and the measured transmission power is 70%.

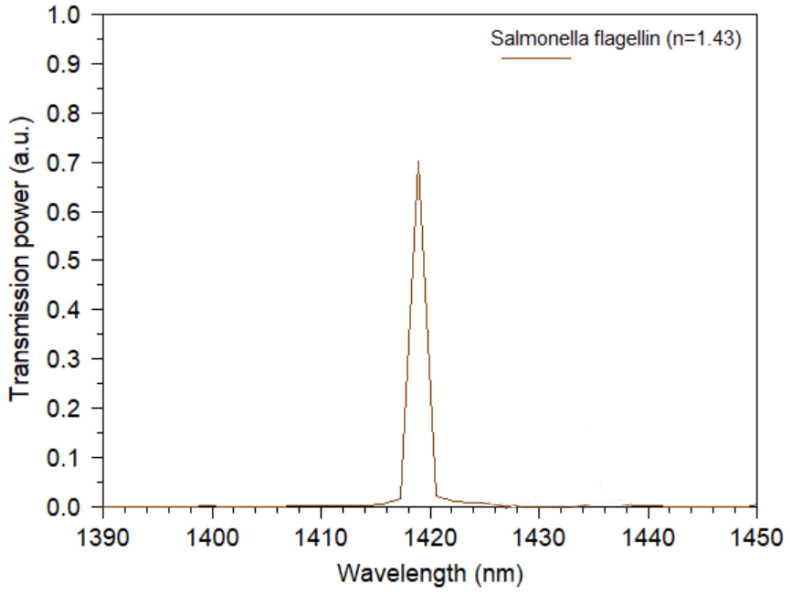

Figure 4.15: Normalized power of biosensor for Salmonella flagellin.

Figure 4.16 illustrates the transmission spectra at the biosensor output for Bacillus subtilis, with refractive index of 1.466 RIU. The resonance wavelength of 1421.5 nm and the measured transmission power is around 100%.

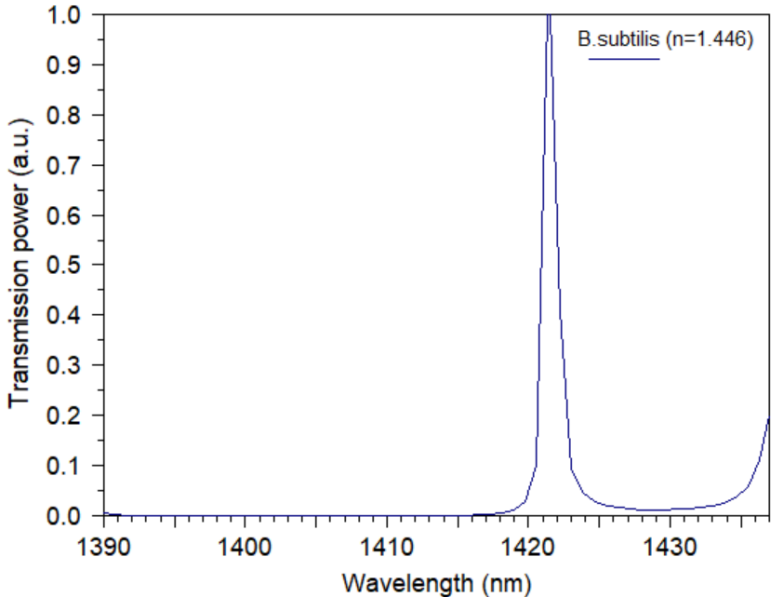

Figure 4.16: Normalized power of biosensor for Salmonella flagellin.

Figure 4.17 illustrates the superposition of transmission spectra measured at the biosensor output for different waterborne bacteria. These bacteria are simulated by refractive indices ranging from 1.3333 to 1.446 RIU.

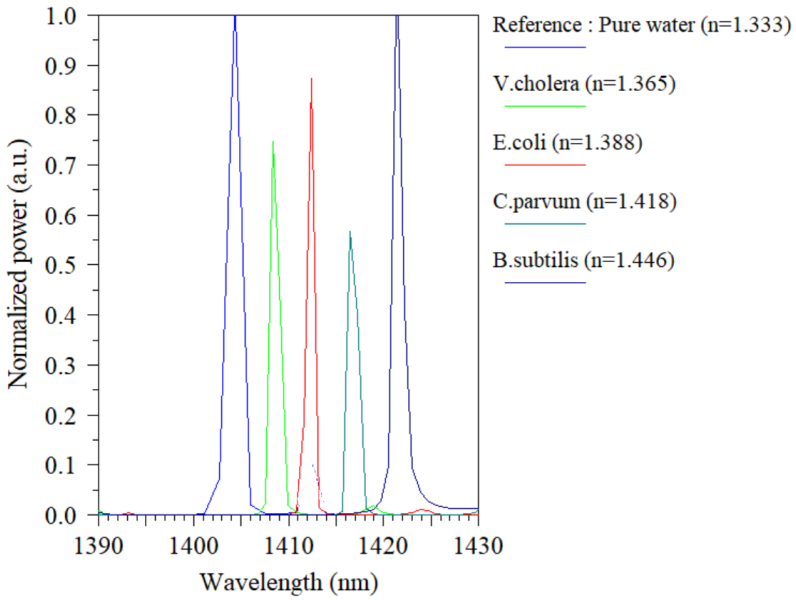

Figure 4.17: Superposition of the transmission spectra for different types of waterborne bacteria.

Table 4.2 presents the simulation results showing that the maximum value of the FOM obtained was 163.65 $(RIU)^{-1}$, with a sensitivity of 147.2 nm/RIU and a quality factor of 1569.4. This value represents our highest performance, with a refractive index of 1.365 RIU. On the other hand, the minimum value of the FOM was 86.581$(RIU)^{-1}$, with a sensitivity of 125 nm/RIU and a quality factor of 702.2. This value represents our lowest performance. The best DL value obtained was $6.1x10^{-4}$ RIU, for a wavelength of 1412.5 nm.

Table 4.2 indicates the summary of the biosensor response for different types of waterborne bacteria . The waterborne bacteria are represented by different refractive indices ranging from 1.333 and 1.446. The quality factor and sensitivity affect the LD. Both increased yield a more reliable LD. Greater sensitivity and quality factor allow for lower concentrations of the analytes to be detected. We achieved a lowest LD value of $6.1x10^{-4}$, which indicates a higher sensitivity promoting the detection of lower analyte concentrations. Our achieved sensitivity was 151.54 nm/RIU, while the quality factor was 1569.4. These results indicate that our technique exhibited the best performance in terms of LD.

Table 4.2: Summarizes the results obtained by the biosensor during the conduction of refractive indices of waterborne bacteria.

Name	RI	$\Delta\lambda_{FWHM}$	λ	Q	S	LD	FOM
Pure water (Ref)	1.333	2.0	1404.4	702.20	-	-	-
V. cholera	1.365	1.3	1408.3	1083.3	125	0.00104	96.153
E. coli	1.388	0.9	1412.5	1569.4	147.29	6.1×10^{-4}	163.650
C. parvum	1.418	1.6	1416.5	885.31	143.52	$1.1x10^{-3}$	89.70
S. flexneri	1.422	1.7	1417.2	833.64	147.19	0.00115	86.581
S. flagellin	1.43	1.7	1419	834.30	151.54	0.00112	89.097
B. subtilis	1.446	1.3	1421.4	1093.38	151.32	$8.5x10^{-4}$	116.390

-1.RI= Refractive index (RIU) -2.$\Delta\lambda_{FWHM}$=Full Width at Half Maximum (nm)-3. λ=Resonance wavelength (nm)-4.Q=Quality factor -5. S=Sensitivity (nm/RIU) -6. DL=Limit of detection (RIU) -7. FOM=Figure of merit $(RIU)^{-1}$

4.5 Linear correlation between resonant wavelengths and refractive indices

Figure 4.18 illustrates the linear correlation assumed between resonant wavelengths and refractive indices. The variation in resonant wavelength with respect to the refractive index is given in the following linear regression equation based on simulated data:

$$\lambda = 150.71 \times n + 1203.18 \tag{4.1}$$

The correlation coefficient value, R^2 = 0.997, indicates a high degree of conformity between the simulated resonant wavelength values and the linear model. The high level of correlation validates the linear approximation in modeling the resonant wavelength shifting.

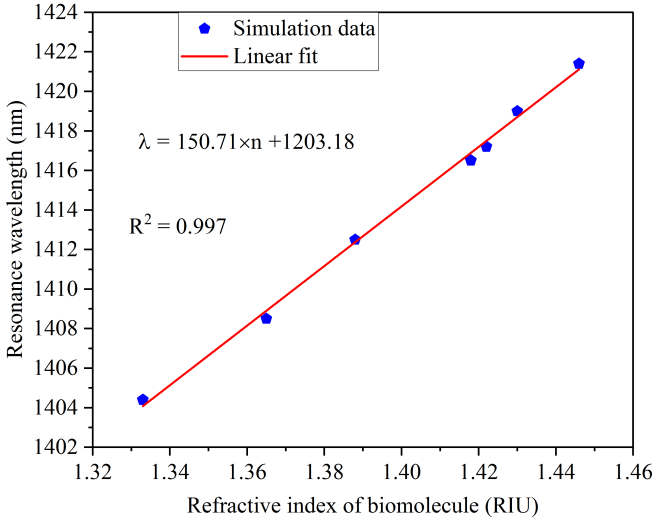

Figure 4.18: Correlation between resonant wavelength and the refractive indices of different bacteria.

4.6 Comparison of the proposed biosensor with different designs with PCs bases

Table 2.3 presents a comparison study between the proposed biosensor and two former photonic crystal-based structures.
The proposed structure here, which is based on a 2D photonic crystal structure, achieves a considerable performance enhancement in terms of sensitivity and detection limit, despite having a relatively moderate quality factor. While the 2024 PC-SPR fiber-based biosensor boasts a very high quality factor of 26595.75, its detection limit has a high value (50.457) which shows a low performance. On the other hand, the 2022 PC-Fiber structure, while simpler, exhibits a much higher detection limit (178.4 UIR) compared to the proposed sensor, which is several orders of magnitude lower (6.1Ö10RIU), indicating greater accuracy in sensing minute refractive index changes.

The suggested structure has a sensitivity of 147.19 nm/RIU, proving its high sensitivity to refractive index change, as needed for the detection of low concentrations of waterborne pathogens. Furthermore, although its quality factor (1569.4) is not the highest among the works compared, it is sufficiently high to allow high selectivity and sharp resonance behavior.

In summary, the proposed 2D PC biosensor demonstrates an optimized and balanced compromise between quality factor, sensitivity, and detection limit, an improvement over the existing designs in parameters that are vital to label-free waterborne pathogen detection.

Table 4.3: Results of previous studies compared to the results obtained.

Ref	Structure	Q	S	DL	RI	FOM	Application
2015 [48]	PC-2D	/	149	/	1.365	/	Waterborne bacteria
2016 [49]	PC-2D	416	1.55	/	1.365	/	Waterborne bacteria
2017 [50]	PC-2D	919	/	/	1.388	100	Waterborne bacteria
2022 [51]	PC-2D	/	35 and 9.4	/	1.365	/	Waterborne bacteria
2022 [52]	PC-Fiber	/	/	178.4	1.365	/	Pathogenic
2024 [53]	PC-SPR Fiber	/	/	50.457	/	/	Pathogenic
Design 1	PC-2D	766.611	148	1.37×10^{-3}	/	82	Waterborne bacteria
Design 2	PC-2D	1569.4	151.54	6.1×10^{-4}	/	163	Waterborne bacteria

-1.Q= Quality factor -2. S=Sensitivity (nm/UIR) -3. DL=Detection limit(UIR)

4.7 Conclusion

We have presented in this chapter a study of a proposed 2D PhC biosensor structure, a dual ring resonator within a square lattice. We optimized first the cavities and the biosensor waveguide so as to obtain a high-quality factor transmission spectrum resonant at 1412.5 nm. We achieved a transmission of 87% and a quality factor of 1767.5 by optimizing the structure. We also demonstrated that the electric field is properly confined in the waveguide and both cavities with negligible losses.

We examinated in detecting waterborne bacteria through affixing biological samples on sensing rods of the biosensor. This design allowed us to track a noticeable variation in transmission intensity from 63% to 100% as the refractive index varied from 1.3333 to 1.43 RIU. we reached a maximum quality factor of 1569.4 and a sensitivity of 151.54 nm/RIU. The provided figure of merit (FOM) values, determinate the efficiency and overall performance of the system, ranging from 86.581 to 163.650 $(\text{RIU})^{-1}$. Moreover, the detection limit was between 0.0011 to 6.1×10^{-4} RIU.
In short, this biosensor appears to be a thrilling device for medical diagnosis based on refractive index change, waterborne pathogen detection, and potential medical discovery in life sciences.

General conclusion

The objective of this dissertation was the design and development of new biosensors for the detection of contaminated water with pathogenic bacteria To achieve this objective, we developed and simulated two distinct configurations of the biosensor. The first was based a single ring resonator, while the second featured an advanced design using dual ring resonators in a two-dimensional photonic crystal (2D PhC) lattice. This work has enabled us to improve the performance of the biosensors through controlled photonic bandgap engineering and shape design of the proposed biosensors, and structural optimization.

The presence of waterborne bacteria in water such as Escherichia coli, Shigella, Salmonella, and Vibrio cholerae are a serious public health issue. Traditional detection methods require specialized instrumentation, and unsuitable for real-time in-the-field detection. Our proposed biosensors offer a strong alternative: it is portable, label-free, and responsive to minute refractive index changes that characterize the presence of target bacteria.

The first biosensor structure utilizing a single ring resonator already exhibited superior performance in terms of resonance sharpness and wavelength shift monitoring. Still, superior performance was achieved by using a dual ring resonator architecture, which significantly enhanced light-matter interaction and led to more discriminable resonance behavior.

The numerical simulations, which were carried out using the Finite Difference Time Domain (FDTD) method, revealed the best sensitivity, quality factor and FoM were obtained for the biosensor designed on the basis of a double resonator. This design, with a sensitivity of 151 nm/RIU, was capable of detecting slight variations in the refractive index corresponding to various bacterial species present in water. A quality factor (Q) of up to 1569, reflecting the tightly bound resonance modes with narrow spectral characteristics. A figure of merit (FOM) of as high as $163(\mathrm{RIU}-1)$, demonstrating the biosensors merit in reconciling sensitivity, selectivity and quality factor. A detection limit (DL) as low as was about $6.1\times10-4\mathrm{RIU}$, confirming the capability of the biosensor in detecting low target analyte concentrations with high precision.

In addition to its strong technical performance, the biosensor is also aligned with two vital axes of national security: health food security. By virtue of the fact that it can detect waterborne pathogens rapidly, inexpensively, and with high sensitivity, the sensor immediately contributes to public health surveillance and food produced water safety assurance. This research addresses two strategic priorities protecting human health and food chain integrity. Moreover, the label-free nature of the sensor avoids the need for external markers, reducing cost and complexity while preserving the biological integrity of the sample. This makes the sensor highly suited for on-site testing, mobile diagnosis, and low-resource environments. Miniaturization also offers the potential to integrate

onto portable lab-on-chip platforms, facilitating real-time water quality analysis. Furthermore, the use of a dual-cavity photonic crystal design enhances detection precision and resonance sharpness, improving both sensitivity and selectivity. Compared to earlier designs that offered lower sensitivity and wider resonance widths, our biosensor provides a marked improvement in both performance and practicality. The structure can be fabricated using existing nanofabrication techniques and is suitable for integration into lab-on-a-chip platforms, thus extending its applicability to real-time, field-based water quality monitoring. This work is a great foundation for extended research on photonic bio-sensing. Future directions for research are:

Experimental validation and demonstration of the proposed structures via nanolithography and photonic integration techniques. Microfluidic integration to facilitate automated sample handling and improved user convenience.

Multianalyte detection capability through multiplex or cascaded resonator configurations.

Exploration of machine learning and artificial intelligence for enhanced optimization of the analysis of biosensor signals and adaptive sensing networks.

Briefly, this thesis represents a promising step forward in the design of optical biosensors, demonstrating that 2D photonic crystal biosensors with dual ring resonators are affective in waterborne bacteria detection. The development from one ring to a dual-ring system demonstrates the way in which judicious photonic engineering can uncover better performance. This innovation can potentially revolutionize water quality testing by providing a convenient, sensitive, and reliable option that is advantageous to our society's health and food security goals.

Bibliography

[1] World Health Organization, "Waterborne diseases," 2019.

[2] UNICEF, "Child mortality from diarrhea." https://www.unicef.org/reports/child-mortality, 2020. Retrieved from https://www.unicef.org/reports/child-mortality.

[3] R. Kumar and P. Singh, "Pcr and elisa methods for pathogen detection: limitations and applications," *Biosensors and Bioelectronics*, vol. 91, pp. 252–260, 2017.

[4] M. Lee and S. Park, "Challenges in real-time water quality monitoring," *Environmental Science & Technology*, vol. 50, no. 4, pp. 2104–2111, 2016.

[5] Y. Chen and L. Zhao, "Label-free optical biosensing based on photonic crystals," *Analytical Chemistry*, vol. 92, no. 15, pp. 10021–10030, 2020.

[6] D. Johnson and X. Wang, "Photonic crystal biosensors: principles and applications," *Sensors*, vol. 19, no. 9, p. 2034, 2019.

[7] E. Yablonovitch, "Inhibited spontaneous emission in solid-state physics and electronics," *Physical Review Letters*, vol. 58, no. 20, pp. 2059–2062, 1987.

[8] J. D. Joannopoulos, S. G. Johnson, J. N. Winn, and R. D. Meade, *Photonic Crystals: Molding the Flow of Light*. Princeton University Press, 2nd ed., 2008.

[9] H. Zhang and C. Lee, "Defect modes in photonic crystals for sensing applications," *Optics Express*, vol. 26, no. 5, pp. 5674–5683, 2018.

[10] J. H. Lee and S. Kim, "Fabrication methods of one-dimensional photonic crystals," *Materials Science and Engineering*, vol. 56, pp. 123–132, 2017.

[11] R. Mahmoud and H. El-Sayed, "Photonic crystal-based biosensors: Recent advances and applications," *Journal of Photonic Sensors*, vol. 9, no. 3, pp. 215–223, 2019.

[12] S. John, "Strong localization of photons in certain disordered dielectric superlattices," *Physical review letters*, vol. 58, no. 23, p. 2486, 1987.

[13] J. D. Joannopoulos, R. D. Meade, J. N. Winn, and P. S. J. Russell, "Photonic crystals: Molding the flow of light," *Nature*, vol. 381, no. 6580, pp. 290–290, 1996.

[14] Y. Desières, *Conception et études optiques de composants micro-photoniques sur matériaux III-V à base de structures à bande interdite de photon*. PhD thesis, Lyon, INSA, 2001.

[15] B. Lombardet, *Etude et réalisation de cristaux photoniques pour l'optique intégrée*. PhD thesis, EPFL, 2005.

[16] B. Wild, *Etude expérimentale des propriétés optiques des cristaux photoniques bidimensionnels et de leur accordabillité.* PhD thesis, EPFL, 2006.

[17] K. Sakoda and K. Sakoda, *Optical properties of photonic crystals*, vol. 2. Springer, 2005.

[18] J. D. Joannopoulos, S. G. Johnson, J. N. Winn, and R. D. Meade, "Molding the flow of light," *Princet. Univ. Press. Princeton, NJ [ua]*, vol. 12, 2008.

[19] S. G. Johnson and J. D. Joannopoulos, "Block-iterative frequency-domain methods for maxwell's equations in a planewave basis," *Optics express*, vol. 8, no. 3, pp. 173–190, 2001.

[20] F. Wen, S. David, X. Checoury, M. El Kurdi, and P. Boucaud, "Two-dimensional photonic crystals with large complete photonic band gaps in both te and tm polarizations," *Optics express*, vol. 16, no. 16, pp. 12278–12289, 2008.

[21] E. Yablonovitch, "Inhibited spontaneous emission in solid-state physics and electronics," *Physical review letters*, vol. 58, no. 20, p. 2059, 1987.

[22] S. Droulias, M. Manousakis, and K. Hizanidis, "Switching dynamics in nonlinear directional fiber couplers with intermodal dispersion," *Optics communications*, vol. 240, no. 1-3, pp. 209–219, 2004.

[23] P. Pottier, C. Seassal, X. Letartre, J. Leclercq, P. Viktorovitch, D. Cassagne, and C. Jouanin, "Triangular and hexagonal high q-factor 2-d photonic bandgap cavities on iii-v suspended membranes," *Journal of lightwave technology*, vol. 17, no. 11, pp. 2058–2062, 2002.

[24] M. Skorobogatiy and J. Yang, *Fundamentals of photonic crystal guiding*. Cambridge university press, 2009.

[25] T. Baba, "Slow light in photonic crystals," *Nature photonics*, vol. 2, no. 8, pp. 465–473, 2008.

[26] X. Fan and I. M. White, "Optofluidic microsystems for chemical and biological analysis," *Nature photonics*, vol. 5, no. 10, pp. 591–597, 2011.

[27] R. Magnusson and S. Wang, "New principle for optical filters," *Applied physics letters*, vol. 61, no. 9, pp. 1022–1024, 1992.

[28] F. Vollmer and S. Arnold, "Whispering-gallery-mode biosensing: label-free detection down to single molecules," *Nature methods*, vol. 5, no. 7, pp. 591–596, 2008.

[29] K. D. Vos, I. Bartolozzi, E. Schacht, P. Bienstman, and R. Baets, "Silicon-on-insulator microring resonator for sensitive and label-free biosensing," *Optics express*, vol. 15, no. 12, pp. 7610–7615, 2007.

[30] K. Jang, *Development of Two-Dimensional Photonic Crystal Hydrogel Sensors for Biomolecular Detection*. PhD thesis, University of Pittsburgh, 2022.

[31] N. Skivesen, A. Têtu, M. Kristensen, J. Kjems, L. H. Frandsen, and P. I. Borel, "Photonic-crystal waveguide biosensor," *Optics Express*, vol. 15, no. 6, pp. 3169–3176, 2007.

[32] B. Cunningham, P. Li, B. Lin, and J. Pepper, "Colorimetric resonant reflection as a direct biochemical assay technique," *Sensors and Actuators B: Chemical*, vol. 81, no. 2-3, pp. 316–328, 2002.

[33] H. Ouyang, C. C. Striemer, and P. M. Fauchet, "Quantitative analysis of the sensitivity of porous silicon optical biosensors," *Applied Physics Letters*, vol. 88, no. 16, 2006.

[34] R. Hadjadj, H. Otmani, M. Boulesbaa, and B. Mekimah, "Effects of physical and geometrical properties on the bandgap of photonic crystals," in *2024 International Conference on Telecommunications and Intelligent Systems (ICTIS)*, pp. 1–4, 2024.

[35] M. E.-F. Hathat, M. Boulesbaa, and S. Gamouh, "Design of new y splitter based on photonic crystal for optical communication," in *2020 1st International Conference on Communications, Control Systems and Signal Processing (CCSSP)*, pp. 552–556, 2020.

[36] M. E.-F. Hathat, M. Boulesbaa, and S. Gamouh, "Design of new y splitter based on photonic crystal for optical communication," in *2020 1st International Conference on Communications, Control Systems and Signal Processing (CCSSP)*, pp. 552–556, IEEE, 2020.

[37] M. E. Hathat, M. Boulesbaa, and S. Gamouh, "Effect of pmma temperature on optical performances of 1 x 2 hybrid photonic crystals waveguide beam splitters," *Journal of nano- and electronic physics*, vol. 15, no. 5, p. 05006(5cc), 2023.

[38] M. Boulesbaa, M. Hathat, A. Bounegab, and O. O. Haddar, "Improvement of optical characteristics of silicon based 1× 3 beam splitter with photonic crystal waveguide," in *AIP Conference Proceedings*, vol. 2440, AIP Publishing, 2022.

[39] F. KIHELI, K. DJEBRIT, and M. BOULESBAA, "Conception des diviseurs de puissance optique 1x2, 1x3 et 1x4 à base des cristaux photoniques," Master's thesis, UNIVERSITÉ KASDI MERBAH OUARGLA, 2020.

[40] M. BOULESBAA, A. AMOUMENE, and I. HALASSA, "Etude et conception des capteurs à base de cristaux photoniques pour la détection de la température," Master's thesis, UNIVERSITY OF KASDI MERBAH OUARGLA, 2022.

[41] M. Boulesbaa, B. Mekimah, and A. Guermache, "Design and analysis of 2d photonic crystals biosensor based on a dual-cavity for brain tissue detection," *Optik*, vol. 322, p. 172160, 2025.

[42] M. BOULESBAA, A. Guermache, and A. Ouali, "Étude et conception de biocapteurs à cristaux photoniques 2d basés sur un guide d'ondes couplé à des cavités," Master's thesis, UNIVERSITY OF KASDI MERBAH OUARGLA, 2023.

[43] M. BOULESBAA, H. N. E. H. Terea, and N. Boudi, "Design and study of a 2d photonic crystal biosensor for detection of blood components," Master's thesis, UNIVERSITY KASDI MERBAH OUARGLA, 2024.

[44] M. BOULESBAA, S. DJEZZAR, and N. HALOUI, "Design and analysis of all-optical photonic crystal logic gates using a combination of yt waveguides," Master's thesis, UNIVERSITY OF KASDI MERBAH OUARGLA, 2024.

[45] N. A. Mohammed, O. E. Khedr, E.-S. M. El-Rabaie, and A. A. Khalaf, "Brain tumors biomedical sensor with high-quality factor and ultra-compact size based on nanocavity 2d photonic crystal," *Alexandria Engineering Journal*, vol. 64, pp. 527–540, 2023.

[46] M. F. Nayan, M. A. Raihan, T. Ahmed, M. H. Fuad, N. A. Zaman, and R. R. Mahmud, "High sensitivity one-dimensional photonic crystal sensor design for waterborne bacteria detection," *Sensing and Imaging*, vol. 26, no. 1, p. 6, 2025.

[47] J. Kim, M. Johnson, W. E. Hill, and B. K. Gale, "Label-free detection and identification of waterborne parasites using a microfluidic multi-angle laser scattering system," *Lab on a Chip*, vol. 15, no. 5, pp. 1060–1067, 2015.

[48] P. Sharma and P. Sharan, "Design of photonic crystal-based biosensor for detection of glucose concentration in urine," *IEEE Sensors Journal*, vol. 15, no. 2, pp. 1035–1042, 2015.

[49] B. Painam, R. Kaler, and M. Kumar, "Photonic crystal waveguide biochemical sensor for the approximation of chemical components concentrations," *Plasmonics*, vol. 12, no. 3, pp. 899–904, 2016.

[50] B. Painam, R. Kaler, and M. Kumar, "On-chip oval-shaped nanocavity photonic crystal waveguide biosensor for detection of foodborne pathogens," *Plasmonics*, vol. 13, no. 2, pp. 445–449, 2017.

[51] R. Kumar, G. K. Bharti, and R. K. Bindal, "Detection and analysis of bacterial water using photonic crystal ring-resonator based refractive-index sensor on soi platform," *International Journal of Electrical and Electronics Research (IJEER)*, vol. 10, no. 4, pp. 826–831, 2022.

[52] E. Haque, A. Al Noman, and F. Ahmed, "Numerical investigation of photonic crystal fiber-based biosensor for pathogens detection in water," *IEEE Access*, vol. 10, pp. 88885–88893, 2022.

[53] A. Banerjee, R. Rahul, J. Thangaraj, and S. Kumar, "High-sensitivity spr fiber-optic biosensor with nano-grating structure for pathogenic bacteria detection in drinking water," *IEEE Sensors Journal*, 2024.